Tectonophysics

Paleoseismological evidence for historical ruptures along the Meduno Thrust (eastern Southern Alps, NE Italy).

--Manuscript Draft--

Manuscript Number:	TECTO15095R1
Article Type:	Research Paper
Keywords:	Active fault; paleoseismology; morphogenic earthquake; applied geophysics; eastern Southern Alps; NE Italy
Corresponding Author:	maria eliana poli, Dr. University of Udine Udine, Udine ITALY
First Author:	maria eliana poli, Dr.
Order of Authors:	maria eliana poli, Dr.
	Emanuela Falcucci
	Stefano Gori
	Giovanni Monegato
	Adriano Zanferrari
	Alessandro Affatato
	Luca Baradello
	Gualtiero Bohm
	Igor Dal Bo
	Enrico Del Pin
	Emanuele Forte
	Stefano Grimaz
	Andrea Marchesini
Abstract:	We carried out new geological, morphotectonic, geophysical and paleoseismological investigations on the Meduno Thrust that belongs to the Pliocene-Quaternary front of the eastern Southern Alps in Friuli (NE Italy). The study area is located in the Carnic Prealps, where a series of alluvial terraces, linked to climatic and tectonic pulses characterises the lower reach of the Meduna Valley. In correspondence of the oblique ramp of the Meduno Thrust, the late Pleistocene Rivalunga terrace, located south of the Meduno village, shows a set of tectonic scarps, only locally modified by human activity. In order to reconstruct the tectonic setting of the area and identify the location for digging paleoseismological trenches, integrated geophysical investigations including electrical resistivity tomography, seismic refraction and reflection, ground penetrating radar and surface wave analyses (HVSR, ReMi and MASW), were carried out across the tectonic scarps of the Rivalunga terrace. Geophysical surveys pinpointed that in correspondence of the oblique ramp, stress is accommodated by a transpressive thrust system involving all the seismo-stratigraphic horizons apart from the ploughed soil. Trenching across the tectonic scarps illustrated the cumulative Meduno Thrust movements during Late Pleistocene-Holocene. Trenches exhibited both shear planes and extrados fracturing showing deformed alluvial and colluvium units. ^{14}C datings of the colluvium units show that the most recent fault movements occurred after 1360 AD and 1670 AD. The very recent age of the deformed stratigraphic units compared with the DBMI15 Catalogue (Rovida et al., 2021), suggests that the 1776.07.10 earthquake (Mw 5.8, Imax=8-9 MCS) could represent the last seismic event linked to the Meduno thrust tectonic activity. This study provided new quantitative constraints improving seismic hazard assessment for Carnic prealpine area.

Abstract

We carried out new geological, morphotectonic, geophysical and paleoseismological investigations on the Meduno Thrust that belongs to the Pliocene-Quaternary front of the eastern Southern Alps in Friuli (NE Italy). The study area is located in the Carnic Prealps, where a series of alluvial terraces, linked to both climatic and tectonic pulses characterises the lower reach of the Meduna Valley. In correspondence of the oblique ramp of the Meduno Thrust, the Late Pleistocene Rivalunga terrace shows a set of scarps perpendicular to the Meduno valley, often modified by human activity. In order to reconstruct the tectonic setting of the area and identify the location for digging paleoseismological trenches, integrated geophysical investigations including electrical resistivity tomography, seismic refraction and reflection, ground penetrating radar and surface wave analyses (HVSR, ReMi and MASW), were carried out across the scarps of the Rivalunga terrace. Geophysical surveys pinpointed that in correspondence of the oblique ramp, stress is accommodated by a transpressive thrust system involving all the seismo-stratigraphic horizons apart from the ploughed soil. Trenching illustrated the Meduno Thrust movements during Late Pleistocene-Holocene. Trenches exhibited both shear planes and extrados fracturing, showing deformed alluvial and colluvial units. ^{14}C datings of the colluvial units show that the most recent fault movements occurred after 1360 AD and 1670 AD. The age of the deformed stratigraphic units compared with the earthquakes listed in current catalogues, suggests that the 1776 earthquake (Mw 5.8, Io=8-9 MCS) could represent the last seismic event linked to the Meduno thrust activity. This study provided new quantitative constraints improving seismic hazard assessment for Carnic prealpine area.

Highlights

We carried out new structural, geophysical and paleoseismological studies on the Quaternary active thrust-front of the eastern Southern Alps (NE Italy).

We demonstrated that the Meduno thrust is an active fault, capable to generate linear morphogenic earthquakes during historical times.

We provided quantitative constraints for the seismic hazard assessment of the prealpine Carnic area.

Paleoseismological evidence for historical ruptures along the Meduno Thrust (eastern Southern Alps, NE Italy).

Maria Eliana Poli (1*), Emanuela Falcucci (2), Stefano Gori (2), Giovanni Monegato (3), Adriano Zanferrari (1), Alessandro Affatato (4), Luca Baradello (4), Gualtiero Böhm (4), Igor Dal Bo (5 formerly at 7), Enrico Del Pin (6), Emanuele Forte (7), Stefano Grimaz (6), Andrea Marchesini (1).

(1) University of Udine; Dept. of Agricultural, Food, Environmental and Animal Sciences – via del Cotonificio 114; 33100 Udine, Italy
eliana.poli@uniud.it; +39 0432 558747
adriano.zanferrari@uniud.it +39 0432 558747
andrea.marchesini@uniud.it; +39 0432 558741

(2) Istituto Nazionale di Geofisica e Vulcanologia (INGV), Via di Vigna Murata 605; 0143 Roma, Italy
emanuela.falcucci@ingv.it; +39 06 518601
stefano.gori@ingv.it; +39 06 518601

(3) CNR - IGG c/o Institute of Geosciences and Earth Resources, Via Gradenigo 6, 35131 Padova, Italy
giovanni.monegato@igg.cnr.it, +39 049 8274177

(4) Istituto Nazionale di Oceanografia e Geofisica Sperimentale, OGS, Borgo Grotta Gigante 42/C – 34010 Sgonico, Trieste, Italy.
aaffatato@inogs.it; +39 040 2140483
lbaradello@inogs.it; +39 040 2140346
gbohm@inogs.it; +39 040 2140295

(5) Agropshere (IBG-3) Institute of Bio- and Geosciences, Forschungszentrum Juelich GmbH
i.dal.bo@fz-juelich.de, +49 2461 61-8663

(6) University of Udine; Polytechnic Dept. of Engineering and Architecture, via del Cotonificio 114 - 33100 Udine, Italy.

stefano.grimaz@uniud.it; +39 0432 558731
enrico.delpin@uniud.it; +39 0432 558732

(7) University of Trieste; Dept. of Mathematic and Geosciences, via Weiss 2 - 34128 Trieste, Italy.
eforte@units.it; +39 040 558 2271

*Corresponding author: eliana.poli@uniud.it

Abstract

We carried out new geological, morphotectonic, geophysical and paleoseismological investigations on the Meduno Thrust that belongs to the Pliocene-Quaternary front of the eastern Southern Alps in Friuli (NE Italy). The study area is located in the Carnic Prealps, where a series of alluvial terraces, linked to both climatic and tectonic pulses characterises the lower reach of the Meduna Valley. In correspondence of the oblique ramp of the Meduno Thrust, the Late Pleistocene Rivalunga terrace shows a set of scarps perpendicular to the Meduno valley, often modified by human activity. In order to reconstruct the tectonic setting of the area and identify the location for digging paleoseismological trenches, integrated geophysical investigations including electrical resistivity tomography, seismic refraction and reflection, ground penetrating radar and surface wave analyses (HVSR, ReMi and MASW), were carried out across the scarps of the Rivalunga terrace. Geophysical surveys pinpointed that in correspondence of the oblique ramp, stress is accommodated by a transpressive thrust system involving all the seismo-stratigraphic horizons apart from the ploughed soil. Trenching illustrated the Meduno Thrust movements during Late Pleistocene-Holocene. Trenches exhibited both shear planes and extrados fracturing, showing deformed alluvial and colluvial units. ^{14}C datings of the colluvial units show that the most recent fault movements occurred after 1360 AD and 1670 AD. The age of the deformed stratigraphic units compared with the earthquakes listed in current catalogues, suggests that the 1776 earthquake (Mw 5.8, Io=8-9 MCS) could represent the last seismic event linked to the Meduno thrust activity. This study provided new quantitative constraints improving seismic hazard assessment for Carnic prealpine area.

Keywords

Active fault, paleoseismology, morphogenic earthquake, applied geophysics, eastern Southern Alps, NE Italy.

Highlights

- We carried out new structural, geophysical and paleoseismological studies on the Quaternary active thrust-front of the eastern Southern Alps (NE Italy).
- We demonstrated that the Meduno thrust is an active fault, capable to generate linear morphogenic earthquakes during historical times.
- We provided quantitative constraints for the seismic hazard assessment of the prealpine Carnic area.

1 - INTRODUCTION

Knowledge of geometric, kinematic, dynamic and chronological parameters of the seismogenetic faults is one of the most crucial topics in an active tectonic region as the eastern Southern Alps (NE Italy). The eastern Southern Alps (ESA) are characterised by destructive earthquakes (Rovida et al., 2021) and, as consequence of high population density, by high seismic risk (Meroni et al., 2008). However, the characterization of the seismogenic sources of these major earthquakes remains poorly constrained especially because Quaternary tectonic activity of the ESA front is related to the SSE-ward propagation of mostly blind thrusts. Despite the region was involved in historical and instrumental destructive earthquakes (for example the 1976 Friuli seismic sequence), until now no evidence of fault surface rupture was reported even for the Susans -Tricesimo thrust, that most of the Authors (see Poli and Zanferrari, 2018 and reference therein) consider the seismogenic source of the 1976 May 6th Friuli earthquake (Mw 6.5). The only possible coseismic ruptures (about 18 cm of cumulative vertical displacement) were pinpointed by Talamo et al. (1977) near Venzone locality and later discussed by Pondrelli et al. (2001), Cheloni et al. (2012; 2014) and Poli and Zanferrari (2018). In such a tectonic context, length of fault segments, slip rate and recurrence interval can be defined only through a multidisciplinary approach based on geological, morphotectonic, geophysical and paleoseismological surveys.

In this work, we present the results of a multidisciplinary investigation on the Meduno Thrust located along the Southalpine front in the Carnic Prealps (NE Italy). We investigated the Late Pleistocene fluvial Rivalunga terrace (Meduno locality) where, in correspondence to the left lateral oblique ramp of the Meduno Thrust, it shows a set of scarps. In order to define the origin of these scarps, we carried out an integrated geophysical survey (Electrical-Resistivity Tomography - ERT, seismic refraction and reflection, Ground Penetrating Radar - GPR, passive seismic and MASW) across these features. The successive digging out of two paleoseismological trenches located where geophysical surveys pinpointed anomalies, allowed us to reconstruct the late Pleistocene – Holocene tectonic activity of the Meduno Thrust, improving the seismic hazard assessment of this sector of the Southalpine region.

2 - GEOLOGICAL AND SEISMOTECTONIC SETTING

The Carnic Prealps belong to the eastern Southern Alps, a polyphase Neogene-Quaternary S-SE-verging fold-and-thrust belt located south of the Periadriatic Lineament (Fig. 1). The eastern Southern Alps, extend from Lessini Mts. to Italian-Slovenian border region and show a complex Alpine tectonic history. After the Mesozoic extension, ESA underwent a polyphase compressional evolution starting from Upper Cretaceous. The oldest structural system corresponds to the WSW-verging, NNW-SSE striking, Upper Cretaceous – Upper Eocene external Dinaric thrust-belt that strongly involved western Slovenia and Friuli (Doglioni and Bosellini, 1987; Vrabec and Fodor, 2006; Ponton, 2010; Zanferrari et al., 2013). Starting from the Neogene, Dinaric structures were involved in the southward propagation of the ESA polyphase, fold-and-thrust belt (Doglioni and Bosellini, 1987; Castellarin et al., 1992; Doglioni, 1992; Castellarin and Cantelli, 2000; Caputo et al., 2010). In particular, from Serravallian to Tortonian, the strong tectonic uplift caused the exposition of the Variscan crystalline basement along the Valsugana Thrust (Zattin et al., 2003; Monegato et al., 2010) and the southward shifting of the ESA foredeep. The progressive tectonic growth of the ESA chain, and the remarkable northward tilting of its foreland, continued during Messinian and Pliocene. A polyphase foreland-verging thrust system, mostly WSW-ENE to SW-NE striking, progressively propagated southwards, causing large amounts of shortening (Doglioni, 1992; Schönborn, 1999) and the progressive filling of the foredeep (Massari et al., 1986; Fantoni et al., 2002; Toscani et al., 2016).

Tectonic activity of the Late Pleistocene-Holocene blind thrusts and the progressive involvement of the Friuli piedmont plain, whose age (Avigliano et al., 2002a) is constrained to the Last Glacial Maximum (LGM, 30-16.5 ka, *sensu* Lambeck et al., 2014), is documented by geological and geomorphological evidence (Paiero and Monegato, 2003; Galadini et al., 2005; Zanferrari et al., 2008a, 2008b; Poli et al., 2009; Zanferrari et al., 2013; Poli et al., 2015; Monegato and Poli, 2015; Patricelli and Poli, 2020).

At present, GPS data (Becthold et al. 2009; Serpelloni et al., 2016) show 2-3 mm/a northward Adria relative motion, generating a maximum NNW-SSE striking compressive stress (sigma 1) in the Carnic prealpine area (where a S-verging fold and thrust belt develops), and NNE-SSW in the Italian-Slovenian border region (Poli and Renner, 2004; Bernardis et al., 2000; Bressan and Bragato, 2009), where the present deformation is accommodated by a system of right lateral strike-slip faults (Fig. 1) (Atanackof et al., 2021; Bajc et al., 2000; Poljak, 2000; Cunningham et al., 2007; Kastelic et al., 2008; Moulin et al., 2014; Falcucci et al., 2018).

Interseismic coupling suggests that the Veneto–Friuli prealpine region accumulates tectonic deformation as elastic strain at seismogenic depth, which will be likely released in future (large) magnitude earthquakes (Barba et al., 2013; Cheloni et al., 2014; Serpelloni et al., 2016; Anderlini et al., 2020).

2.1 – Seismicity

The eastern Southern Alps have been struck by numerous earthquakes with Mw between 6 and 7 in the past (Rovida et al., 2021). In particular, five moderate to strong historical and instrumental seismic events struck the Carnic Prealps causing high damage and many casualties (Table 1). Conversely, since the destructive earthquakes that hit Friuli on 1976 (May 6th and September 15th with Io 10, Mw 6.5 and Io 8-9, Mw 5.9 respectively), the Seismometric Network managed by the National Institute of Geophysics and Oceanography (OGS, Trieste), recorded only a few significant events in the Carnic Prealps: the 1986/08/29 Mt. Pramaggiore earthquake (ML 4.0); the 1996/04/13 Claut earthquake (ML 4.3 Bernardis et al., 1996) and the 2012/06/09, Barcis earthquake (ML 4.0).

3. METHODS

In order to identify the morphological anomalies on the Rivalunga terrace, we firstly analyzed the digital elevation model (DTM) made available by the Regione Friuli Venezia Giulia (http://irdat.regione.fvg.it/CTRN/ricerca-cartografia/). The DTM is a 1 m square grid obtained from TIN elaboration of LIDaR ground classified data from helipcoter fly, density average of 4 points per square meter. Accuracy of about ten centimeters at altitude, the elevation is corrected according with some geometric leveling benchmarks and a reference geoid.

Then, integrated geophysical investigations (i.e. Electrical Resistivity Tomography - ERT, seismic refraction tomography, seismic reflection, Ground Penetrating Radar - GPR, passive seismic and MASW), were carried out across the scarps on the LGM Rivalunga terrace. To improve the signal-to-noise ratio and to obtain stack images, all seismic reflection profiles were processed with standard processing using Focus software (PARADIGM). Seismic tomography was computed inverting the first travel times arrivals (Böhm et al., 2013), picked in the pre-stack seismic domain, by using the SIRT algorithm (Stewart, 1993) and the staggered grids methods (Vesnaver and Böhm, 2000). ERT supported other geophysical techniques: we compared the dipole-dipole array to the other ones, in order to look for a better lateral resolution and to map the vertical structures.

Concerning the GPR, the electromagnetic velocity field used for static (topographic) corrections, depth conversion, and migration was estimated by manual and semi-automatic diffraction hyperbolas fitting. Geometry assessment and checking was done exploiting QGIS open source suite and two plugins, namely: QChainage and Point Sampling Tool. 2-D migration was done by applying Stolt f-k algorithm, which performs well for smooth velocity fields, like in the present case. GPR processed dataset was imported in Petrel software (Schlumberger) for data interpretation and integration.

Concerning the Passive Seismic, we adopted a combined use of surface wave analysis (HVSR, ReMi and MASW). The three methods were used with an integrated approach to characterize the entire site. In particular, the horizontal to vertical spectral ratio (HVSR) technique allows to identify site fundamental frequencies (Carniel et al., 2008) while the refraction microtremor (ReMi) technique and the multichannel analysis of surface wave (MASW) technique are used to estimate the shear wave velocities in depth (Louie, 2001; Park et al., 1999).

Data acquisition and processing flow of the adopted investigations are summed up in Table 2.

Based on the geophysics results we selected two trench sites across the Meduno Thrust. Trenches were dug across the "original" fault scarp, as the present-day one has been slightly altered from the human activity. Specifically, the fault scarp has been rectified and advanced with respect to its original position owing to anthropogenic accumulation of material at the base of the scarp, probably for agricultural practices. Moreover, it is also worth noting that no "anomaly" potentially attributable to faulting has been detected by the geophysical investigations performed across the present-day toe of the scarp. Furthermore, the base of the present-day scarp is strongly affected by human action and land arrangements for agricultural activities are clearly evident.

Trenches walls were equipped with a 1m x 1m sting grid and logged at a scale of 1:10. Radiocarbon dating was performed by BETA Analytic on charcoal and bulk organic carbon samples.

4. – QUATERNARY TECTONIC ACTIVITY OF THE STUDY AREA

During the last decades, matching geological and morphotectonic surveys with the interpretation of a set of seismic lines (gently provided by ENI, Exploration & Production Division), Zanferrari et al. (2008b), Poli et al. (2009), Monegato and Poli (2015), Poli et al. (2015), produced a detailed structural framework of the SW-NE to WSW-ENE trending, foreland-verging thrust-system of the Pliocene-Quaternary front in the Carnic Prealps (Fig. 2 and Fig. 3).

In particular, this work focuses on the Meduno Thrust, which is part of the Mt. Jouf Thrust-System, consisting of a set of active reverse faults (Monte Jouf, Maniago Libero, Meduno and

Solimbergo Thrusts in Fig. 2) which border the reliefs between Maniago and Meduno and propagate in the LGM piedmont plain.

4.1 – Monte Jouf Thrust (MJ)

The Mt. Jouf Thrust consists of a NW-dipping reverse fault that crops out for about 12 km from Maniago to Meduno (Fig. 2). The Mt. Jouf Thrust gives rise to a strong morphological elevation (i.e. the Mt. Jouf karstic massif) which rises up on the piedmont plain about 1000 metres. In the hanging-wall, a S-verging recumbent frontal anticline (with the axis dipping about 15° toward the NE) involves both Mesozoic (Cellina Limestone and Monte Cavallo Limestone) and Cenozoic (Scaglia Rossa Fm. and Clauzetto Flysch) units (Stefani, 1982; Zanferrari et al., 2008b). Towards the East, MJ ends on the Toppo Tear Fault (TO in Fig. 2), which transfers deformation to the South. Toward the West, slip decreases because of the presence of another thrust segment with an *en-echelon* relationship (the Polcenigo-Montereale Thrust, PM in Fig. 2).
The MJ shows scattered evidence of Pliocene-Quaternary activity: near Maniago, it involves the Lower to Middle Pleistocene alluvial deposits (respectively Maniago Conglomerates and Maniago Gravels in Zanferrari et al., 2008b). North of Meduno, near Valle locality (Fig. 4), MJ involves the Pliocene(?) Del Bianco Conglomerate (Feruglio, 1929; Venturini et al., 2013). Northward, MJ cuts the WSW-verging, low-angle Paleogene Dinaric frontal ramp of the Mt. Ciaurlec Thrust (MC; Fig. 2) (Zanferrari et al., 2008b; Ponton, 2010).

4.2 – The Maniago Libero Thrust (ML)

The NE-SW trending, SE-verging Maniago Libero blind Thrust develops in the footwall of the Mt. Jouf Thrust. ML extends for about 4 km from Maniago Libero to Maniago (Fig. 2) and strongly involves both the Montello Conglomerate (Upper Miocene) and the Plio-Quaternary conglomerates of the Friuli Supersynthem in a series of NE-SW trending tectonic slices.

4.3 – The Meduno Thrust (ME)

The Meduno Thrust consists of a mostly buried NE-SW trending, SE-verging medium to high angle thrust, extending for about 8 km from Fanna to Meduno (Fig. 2). It gives rise to a series of outcropping NE-SW trending tight folds involving both the Lower Eocene emipelagic and turbiditic deposits and the Miocene terrigenous units (Fig. 2 and Fig. 3). Toward the SW, ME tectonic unit overlaps the ML Thrust along the Colvera River (Fig. 2). Toward the South, a frontal splay of Meduno Thrust (i.e. ME_1 in Fig. 2 and in Fig. 5) displaces the bottom of the Pliocene-Quaternary succession. Near Meduno (Ponte Maraldi locality in Fig. 2 and Fig. 6) ME

crops out, giving rise to a left lateral oblique ramp (N280°/70° dipping), involving both the Upper Miocene Montello Conglomerate and the uppermost Pleistocene alluvial gravels with an estimated verticalthrow rate of about 0.6 mm/a for the last 30 ky (Monegato and Poli, 2015). To the East, Meduno Thrust closes on the Toppo fault (Fig. 2).

4.4 – The Solimbergo Thrust (SO)

The Solimbergo Thrust is a WSW-ENE striking, S-verging arcuate blind thrust running under the Late Pleistocene sequence of the piedmont plain between the Colvera and the Cosa creeks (Fig. 2). Concerning the morphotectonic features, Zanferrari et al. (2008b) showed that SO gently warps the topographic surface carved in the LGM gravels North of Sequals (Fig. 2). Moreover, in correspondence of this bending feature, along the left site of the Meduna River, the weakly cemented gravels of the Friuli Supersynthem (likely Middle Pleistocene in age, Zanferrari et al., 2008b) are uplifted and tilted toward the North of about 10°.

5 – GEOPHYSICAL SURVEY

In the lower reach of the Meduna valley, the progressive entrenching of the Meduna River into the Miocene and Quaternary successions created a series of terraces with steep riverside scarps (Monegato and Poli, 2015). The age of the depositional surfaces was inferred from regional stratigraphic setting and the most recent units are related to the aggradation of the Meduna alluvial fan (Avigliano et al., 2002a; Zanferrari et al., 2008b) during the last two glacial periods. In detail, the Meduno terrace was ascribed to the Middle Pleistocene, while the Rivalunga terrace to the Last Glacial Maximum (Monegato and Poli, 2015). Both terraces show a high scarp of 15m and 7m respectively (Fig. 7), whose direction is perpendicular to the Meduna incision. Integrated geophysical investigations were carried out across the scarps on the LGM Rivalunga terrace (Fig. 7) with the aim to: 1) define the origin of these morphological features, 2) reconstruct the tectonic architecture of the Meduno Thrust, 3) define the fault trace, 4) identify the location for digging the paleoseismological trenches.

In the following we describe the results of the different geophysical techniques adopted in this work (see Chapter 2 and Table 2 for details).

5.1 - Seismic tomography, reflection seismic and electrical resistivity tomography

Seismic and geoelectrical surveys, recorded along the same acquisition paths, investigated the Rivalunga terrace by means of three more than 200 m-long, WNW-ESE to NW-SE striking

profiles (S1-line, S3-line and S4-line in Fig. 7). An additional WNW–ESE profile (S2_line in Fig. 7) was carried out in correspondence of the left side of Meduna River where geological field observations pinpointed undisturbed sedimentation.

In the following, we present the interpretation of the seismic reflection, seismic refraction tomography and electric resistivity tomography for each profile: S2 line (Fig. 8), S1 line (Fig. 9), S3 line (Fig. 10) and S4 line (Fig. 11). Moreover, in order to clarify the geological setting of the study area, we built up for each geophysical profile the relative geological cross section including the erosional scarp and the Meduna riverbed (Fig. 8d: BB' geological section; Fig. 9d: AA' geological section; Fig. 10d: CC' geological section, Fig.11d: DD' geological section). For location see Fig. 7.

In order to understand the geological setting of the Rivalunga terrace, we compare the results of the seismic survey of S2-line (Fig. 8) with the geological field observations along the left side of Meduna River, South of Ponte Maraldi (i.e. the footwall of the Meduno Thrust in Fig. 7). Here seismic reflection (Fig. 8a) and seismic tomography (Fig. 8b) confirm the un-deformed setting of the sedimentary succession. In particular, seismic tomography identified three different sub-parallel seismo-stratigraphic horizons: the shallow horizon (Vp 1000 m/sec) is about 25-30 m-thick. Based on field observations, it corresponds to the LGM gravels of the Meduna River that form the Rivalunga terrace (Monegato and Poli, 2015). A second sedimentary body is characterised by Vp 2000-2500 m/sec and corresponds to pre-LGM deposits (gravels and conglomerates) of the Friuli Supersynthem (Zanferrari et al., 2008b). The deepest horizon (Vp about 3000-3500 m/sec) corresponds to the Upper Miocene conglomerates outcropping along the right side of the Meduna river in correspondence of Ponte Maraldi (Fig. 6). ERT (Fig. 8c) confirms the un-deformed setting of the left side of Rivalunga terrace: along this section, no abrupt resistivity contrast was observed. On these bases, we reconstructed the geological setting of the S2 line in Fig. 8d.

On the contrary, the others geophysical profiles carried out on the LGM Rivalunga terrace show a complex structural arrangement across the morphological scarps. Seismic profiles (Fig. 9a, Fig. 10a and Fig. 11a) pinpoint a high angle transpressive fault-system that displaces the Quaternary succession. Across the tectonic scarp faults propagate towards the surface, involving all the seismo-stratigraphic horizons. Seismic tomography (Fig. 9b, 10b and 11b) and electro-resistivity investigations (Fig. 9c, 10c and 11c) confirm this interpretation showing anomalous distributions of the velocities and sharply changes in resistivity values along the tectonic scarps.

Concerning the interpretative geological cross sections obtained matching surface geology and geophysical results (Fig. 9d, 10d, and 11d), we can observe that: i) the Quaternary sediments seal the synclinal fold that involves the Upper Miocene strata; ii) tectonic activity of the Meduno

transpressive fault-system conditioned deposition of the Quaternary deposits: crossing the scarp, both pre-LGM and LGM deposits strongly thicken southward, as already observed by Monegato and Poli (2015); iii) Upper Pleistocene-Holocene sediments are involved in the tectonic activity of the Meduno Thrust.

5.2 - Passive seismic investigations

Passive seismic survey concentrated on the western edge of the Rivalunga terrace (Fig. 12), highlighting the first 20 – 40 m–deep of the stratigraphic succession. In particular, MASW and Remi profiles (Profiles M and V in Table 3) intersect S3 line (Fig. 12), pinpointing the presence of three main sedimentary layers (Table 3).

Moreover, using HVSR technique, we extended the survey across the fault scarp in order to investigate the variations of H/V spectra and fundamental frequencies (Fig. 12 and Fig. 13). Proper design of ambient noise measurement points and interpretations were carried out for a rapid check of site and sub-soil characteristics (Carniel et al., 2008; Grimaz et al., 2014). The natural microtremor was recorded along two alignments of measurement points across the Rivalunga terrace (HV1 and HV2 profiles in Fig. 13a). The major changes of natural frequency were identified across the tectonic scarp, where the comparison between the results of the ReMi and MASW surveys and fundamental frequencies indicates a significant increase in thickness of the stratigraphic layers (Fig. 13 b, c).

5.3 - GPR

GPR survey allowed a subsurface imaging with decimetric resolution reaching a maximum depth of 6 m. In Fig. 14, two GPR profiles along the paleoseismological trenches (location in Fig. 7) are reported, while in Fig. 15 a portion of the interpreted GPR line-4 is shown with different attributes. GPR attributes have been used since recent years for seismological purposes allowing to get quantitative data in addition to an improved high-resolution subsurface imaging (McClymont et al., 2008; Beauprêtre et al. 2012; Ercoli et al., 2014, 2015; Dal Bo, 2015). The overall data quality is quite high allowing to interpret in the western sector (hanging-wall) several horizons with increasing dips (0°-15°) toward east-south east (H2, H3, H4 and H5 in Fig. 15). Such horizons are abruptly interrupted in a zone located at about 10 to 25 m from the topographic scarp. This area has a chaotic GPR signature with several diffractions and with only few sub-horizontal reflectors having an overall low lateral continuity (H6 in Fig. 15). In the shallower portion (first meter), there are sub-horizontal continuous reflectors (H0 and H1 in Fig. 15). All that structures, even at a different resolution level, match very well the stratigraphy

highlighted by the paleoseismological trenches (Fig. 16 and Fig. 17). This is quite apparent by comparing the MED_EAST trench (Fig. 17), with the portion of GPR profile previously acquire just few meters apart (Figs. 7 and 15).

6 - PALEOSEISMOLOGICAL TRENCHES

According to morphotectonic and geophysical results, we dug two trenches (MED_WEST and MED_EAST, Fig. 16 and Fig. 17 respectively) on the Rivalunga terrace (Fig. 7). We crossed the trace of the Meduno fault, as showed by geophysical investigations.

The excavations exposed a continental sedimentary sequence, which mainly consists in alluvial and colluvial deposits. Six stratigraphic units have been distinguished from top to bottom (Fig. 16 and Fig. 17) and described below.

Unit 1: colluvial deposit made of brownish massive sandy silt containing centimetre-size carbonate sub-rounded-to-rounded pebbles. The unit unconformably overlays the older units through an erosional surface.

Unit 2: anthropogenic deposit made of decimetric-size carbonate blocks; this unit is the product of man-made regularization of the scarp.

Units 3 and 4: colluvial deposits made of brownish massive sandy silt containing centimetre-size carbonate sub-rounded-to-rounded pebbles. An erosional surface separates the two units.

Unit 5: sandy gravels, sub-rounded-to-rounded, clast-supported and cross-bedded. Basal boundary is erosive and unconformably covers the underlain deposits. The unit is interpreted as an alluvial deposit of the Meduna River before its trenching at 18.5 ky (Monegato and Poli, 2015).

Unit 6: coarse-grained gravels, clast-supported, crudely bedded to cross-bedded, with a layer of clast-supported massive diamicton, with sub-rounded boulders and sandy matrix. We interpret this unit as fluvial deposition, with gravel-bar migration and occurrence of debris-flow events of the Meduna River, related to the last glacial period of the Late Pleistocene (Monegato and Ravazzi, 2018) having the climax during the LGM.

Both units 5 and 6 show an overall bedding gently dipping southwards, consistent with the flow direction of the Meduna River. Local but relevant variations of the attitude of the gravel layers were observed in the southern sector of both trenches. These variations, represented by portions of the gravel with a local much higher dip angle and/or with an evident counter-flow attitude, are associated to deformation features described below.

We correlated the units across the trenches by considering: *i*) the sedimentological and stratimetric characteristics of the units; *ii*) the stratigraphic relationship among different units, (especially with respect to alluvial units 5 and 6; see below); *iii*) the comparable depth of the units with respect to the topographic surface; and *iv*) the short distance between the two trenches (on the order of two hundred metres).

In order to obtain chronologic constraints for the units deposition, five samples (charcoals and a bulk of organic matter) have been collected from the sedimentary sequence for radiocarbon dating (dating made by BETA ANALYTIC laboratory); the results of the analyses are summarized in Table 4.

It has to be noted that the obtained ages all define a *post quem* age of the unit deposition, since the dated samples were contained within alluvial and colluvial sediments. Therefore, we have considered only the most recent ages achieved for each unit in terms of chronology of the deformation, as described below. It is also worth noting that the charcoal contained within Unit 6, aged at 35920 ± 280 BP confirms the unit deposition during the Last Glacial Period before the LGM. The definition of the chronological constraints for unit 3 has been obtained by dating charcoals (samples MEDU_EST_4, _10 and _12, see Table 4). Dating of the organic bulk (sample MEDU_OVEST_bulk_2) has been performed to support the ages obtained from dating the charcoals. In particular, we feel confident in correlating the two colluvial bodies across the two trenches because: 1) they are comparable by lithology and sedimentological characteristics, belonging to the reworking of the poorly developed soil characterising the post-LGM of the piedmont plain (Avigliano et al., 2002b; Zanferrari et al., 2008b); 2) they are in the same geometric and stratigraphic relation with the older and younger units; 3) even though the trenches are about 250 m apart, the colluvial deposits are related to the very closely spaced morphological features related to the same tectonic feature, that is the trenched scarps; there are no other source zones (i.e. coalescent fluvial or stream incisions; landslide scarps), from which the colluvial units could have been fed in different periods; 4) even if the obtained ages may seem different for unit 3 in the two trenches, it has to be considered that the age obtained is not the age of deposition of the colluvial units, as the charcoal ages are the terminus *post quem* for the units deposition; 5) it must be taken into account that the dating obtained from unit 3 in trench MEDU WEST derives from dating of charcoals, whereas the dating obtained from unit 3 in trench MEDU EAST derives from dating of a bulk of the organic matrix of the colluvial body; therefore, the dating are not fully comparable, owing to different dated organic material.

Therefore, considering the other observations above described, it is likely that the two sedimentary bodies can be included in same stratigraphic unit (unit 3), formed during the same climatic-depositional phase (i.e. after the starting of the post-glacial pedogenesis of the terrace).

411

412 **6.1 – Paleoseismological trenching results**

413 The analysis of the walls of the trenches permitted the identification of some shear planes
414 showing reverse kinematics, observed close to the fault scarp (Fig. 16d and Fig. 17f).
415 The shear planes were responsible for the displacement of almost all of the stratigraphic units.
416 Thrusting of the stratigraphic units determined a shear fabric, testified by the local superposition
417 of older on younger units and by dragged and aligned clasts that evidence the attitude of the fault
418 planes. In details, we interpreted these latter as shear zones because of the arrangement of the
419 pebbles. Indeed, the pebbles showed the same attitude, i.e. counter-slope dipping, which is
420 opposite to that in the other sectors of the trenches, i.e. downslope dipping, the latter testifying to
421 the natural aggradation of the alluvial fan. Therefore, the abrupt change in the pebble attitude,
422 and the absence of any structure that could testify cross-bedding set, suggest its post-depositional
423 modification (Fig. 16b, c; Fig. 17a, b, c, d; Fig. 18a, b, c).
424 Concerning the superposition of older on younger units, this is visible in both trenches. In
425 MED_WEST, at least two fault planes (dipping N270°/30° and N310°/80°) superposed units 5
426 and 6 on unit 4, respectively (Fig. 16b and Fig. 18 a, b, c) and unit 4 on unit 3 (Fig. 18d, e, f). In
427 MED_EAST unit 5 is thrusted on unit 3 by means of a shear plane dipping 270°/40° (Fig. 17c, d,
428 e).
429 Further evidence that testifies to the presence of a shear zone is the thickening of unit 3 toward
430 the South and, perhaps, the warping (upward convexity) of the contact between unit 3 and the
431 underlying units in proximity of the surface scarp clearly visible in MED-WEST (Fig. 16).
432 The localized bending, the anomalous lateral contacts between units 3-4-5 and the rotated and
433 realigned clasts on shear surfaces, allow to rule out that these geometrical features relate to
434 primary sedimentary phenomena. On the other hand, these features allow to define that the
435 observed setting is due to reverse kinematics.
436 In terms of displacement events, the relationship between the fault planes and the sedimentary
437 units permitted us the identification of two subsequent events occurred along two different fault
438 zones (named as F1 and F2, Fig. 16, Fig. 17 and Fig. 18). Concerning MED_WEST, the oldest
439 event (E2) is testified by the displacement of units 6-5 along F1 (Fig 16b; Fig. 18 a, b, c). The
440 fault plane was sealed by the overlaying unit 3 which, in turn, was displaced and deformed by F2
441 during a subsequent event (E1) (Fig 16b; Fig. 18 d, e, f). These events have been recognised in
442 both trenches. In particular, in trench MED_EAST, E1 was responsible for about 20 cm vertical
443 reverse offset (Fig. 17c, d, e). Even if the displacement caused by E1 appears less evident in the
444 trench MED_WEST, the observations made along the walls of the trench MED_EAST
445 corroborated the event identification. Here the event is testified by the offset affecting the base of

unit 3 corresponding, moreover, with the presence of rotated pebbles belonging to unit 5, placed in lateral contact with the colluvial unit 3 (Fig. 17c, d). Given the erosional nature of the contact between units 5-3, the pebbles of unit 5 "injected" into unit 3 cannot be explained with sedimentary processes, without invoking a post-depositional deformation.

Moreover, in the northern sector of trench MED_WEST, we identified secondary deformation features characterised by an extensional kinematics (Fig.16b and Fig. 19a, b, c); these consist in subvertical shear planes oriented N30° to N90°. Importantly, these shear planes ended downwards at roughly 3-4 m-depth (Fig 19c). Based on this, we interpret these features as fractures that affected the exposed units in concomitance of a surface rupture seismic event. Indeed, taking into consideration the transpressive tectonic features described above, we can infer that these features are moment bending fractures (MBF) associated to the bending of the shallowest deposits during the compressive deformation (e.g. Livio et al., 2019).

Also, as defined by McCalpin (2009, and references therein), bending-moment faults (extrados fractures) are secondary to the thrusts that underlay folds and form suddenly as brittle-deformation structures during thrust-generated flexure of the anticline, as the result of an instantaneous deformation. The fact that they display a very high angle dip and that they affect loose sediments (gravel) indicate that their formation is very rapid, and not therefore relatable to creep movements of the compressive structure (see McCalpin, 2009 on this topic).

We identified two deformation events along these extrados-related features (Fig. 19). The oldest event occurred after unit 6 deposition and before unit 5 deposition. A subsequent event displaced unit 5 prior to unit 1. This latter event could be associated to the above described event E1 that we recognised in the same trench along the reverse fault zone F2.

The radiocarbon ages allow us to chronologically constrain the two recognised tectonic events. The youngest event (E1) occurred subsequently to the deposition of unit 3. This indicates that E1 took place after 1470–1650 AD; 1470–1650 AD; 1330–1440 AD (calibrated 2 sigma), i.e. after the 15^{th}-17^{th} century AD, based on the youngest radiocarbon age defined for unit 3.

The lack of chronological constraints for unit 1 deposition prevented to bracket the age of E1. The collected evidence permit to only state a "*post-quem*" age for E1, that occurred after unit 3 deposition, i.e. after 1470–1650 AD.

As for E2, we can only state that it occurred after the deposition of the Uppermost Pleistocene-Holocene unit 4 (not dated) and before the deposition of unit 3.

7 - DISCUSSION AND CONCLUDING REMARKS

The Pliocene-Quaternary external front of the eastern Southern Alps in Carnic Prealps consists in a S-SE foreland verging thrust-system that propagates in the LGM piedmont Friuli plain by means of mainly blind thrusts, which gave rise to widespread morphotectonic evidence of recent deformations. Despite the region was involved in historical and instrumental destructive earthquakes (for example the 1976 Friuli seismic sequence), until now no evidence of fault surface rupture was reported even for the Susans -Tricesimo thrust, that most of the Authors (see Poli and Zanferrari, 2018) consider the seismogenic source of the 1976 May 6th Friuli earthquake (Mw 6.5).

In this work we studied, by means of a multidisciplinary approach, the morphotectonic and seismotectonic characteristics of a southern splay of the Mt. Jouf Thrust-System, i.e. the Meduno Thrust, a NE-SW striking, SE-verging medium angle reverse fault that runs at the base of the Carnic Prealps in Friuli. Near Meduno, it changes in strike giving rise to a NNE-SSW steep oblique ramp with a late Pleistocene-Holocene throw rate of about 0.6 mm/a (Monegato and Poli, 2015).

In correspondence of the oblique ramp, the LGM Rivalunga terrace shows an alignment of about NNE-SSW to NE-SW striking, 600 m-long and 1-to-7 m high scarps. Despite the scarps were often modified with respect to their original position owing to agricultural practices, all the different geophysical investigations, even at a different resolution level, show peculiar geophysical signatures moving close these morphological anomalies. In particular, interpretation of seismic refection profiles confirm that deformation is accommodated by a transpressive fault-system that involves also the Late Pleistocene-Holocene sedimentary succession. Tectonic activity of the Meduno transpressive fault-system conditioned deposition of Quaternary succession: crossing the scarp, both pre-LGM and LGM deposits strongly thicken southward. Also close to the topographic surface, GPR surveys highlight apparent lateral interruptions and dip variations of imaged horizons, as well as high angle discontinuities reaching very shallow depths (i.e. less than 1 m) below the present surface.

Moreover, the digging of two paleoseismological trenches across the geophysical anomalies observed close to the scarps showed the following:

- all the stratigraphic units, with the exception of the ploughed soil, record tectonic deformation;
- both superposition of older on younger units and flat-clasts frequently dragged and realigned on shear surfaces, testify tectonic deformation;
- strike of faults and fractures is consistent with the direction of the oblique thrust ramp;

- moving close the scarps, the stratigraphic units give rise to an anticlinal warping, where also the historical colluvial units notably thicken towards the thrust front. This arrangement is coherent with the deformation visible in the seismic reflection profiles where a transpressive structure develops along the oblique ramp.
- the extrados fractures in the norther portion of the MED_OVEST, represent a structural assemblage coherent with the activation of a reverse fault (Nurminen et al., 2020).
- chronological constrains (Tab. 4) bracket in time the two distinguished faulting events: the oldest (E2) occurred after the deposition of unit 4 (post-LGM, likely Uppermost Pleistocene-Holocene colluvium) but it was sealed by unit 3 that was dated as past 1470–1650 AD; 1470–1650 AD; 1330–1440 AD (2sigma calibrated ages); the younger (E1) occurred after the deposition of unit 3, but is sealed by unit 1 (that was not dated).

Concerning the potential seismogenic sources of this portion of the ESA front, this study confirms the Quaternary tectonic activity of the Mt. Jouf Thrust-System. In particular, our results agree with the Plio-Quaternary tectono sedimentary reconstruction of this sector of the Carnic Prealps proposed by Monegato and Poli (2015). Studying the fluvial terraces of the Meduna River, these Authors observed that the Mt. Jouf Th. deformed Pliocene (Fig. 4) and Lower-Middle Pleistocene deposits, but it did not involve the LGM terrace which, on the contrary, was displaced by the Meduno Th. (see Fig. 6 of Monegato & Poli, 2015 and Fig. 6, of this paper). Paleoseismological evidence seems to confirm the significant tectonic activity of the Meduno thrust during Late Pleistocene – Holocene, confirming that the tectonic activity of the Meduno Th. postdates the Neogene-Quaternary S-verging fold and thrust belt affecting the Miocene Molasse. On these bases, we can hypothesize that, starting from the Upper Pleistocene, deformation has been transferred from the Mt. Jouf Th. to the Meduno one.

In order to identify the historical earthquakes that could have generated superficial faulting in the Meduno area, we analysed the available historical seismic catalogue (Rovida et al., 2021), gathering the earthquakes with Mw≥ 5.8 occurred after 1650 AD in the Meduno neighbouring region. Considering the completeness of the catalogue in the last three centuries as for major seismicity (e.g. Stucchi et al., 2004), the only known post-17th century AD earthquake with a magnitude large enough to possibly deform/affect the topographic surface in the study area is the Prealpi Carniche earthquake (Mw: 5.8; Io 8-9) occurred in 1776/07/10, which affected the area of Meduno, as reported by the database DBMI15 (Rovida et al., 2021; Fig. 20). Even if the total number of data-points showing medium-high damage is little (9 data- points), probably because the area is sparsely populated, epicentral zone is well defined and is mainly located in the hanginwall of the Meduno Th. This study allowed us to give quantitative constraints on

546 geometry, kinematics, dynamics and chronology of the Meduno Thrust, useful to improve
547 seismic hazard assessment of the western Friuli region. They are summarised in Table 5.
548 Multidisciplinary approach demonstrated that the Meduno Th. could generate morphogenic
549 earthquakes, i.e. seismic faulting events that are capable of generating or modifying the surface
550 morphology instantaneously and permanently (Caputo, 1993, 2005). For the first time we
551 demonstrate that at the front of the eastern Southern Alps, where usually thrusts are blind, some
552 seismic events may generate surface rupture.
553 In general, the fault displacement hazard of normal and strike-slip faults has been much more
554 studied than that of thrust faults. Only a few works deals with this argument. In particular,
555 Boncio et al., (2018), focused on the rupture zone of reverse or oblique faults suggesting
556 example from different world areas. In this work some reverse/oblique earthquakes (Coalinga,
557 1983/06/30 – Mw5.4; and Marryat Creek 1986/03/30, Mw 5.8) showed evidence of maximum
558 displacement of 0,64 m and 1,3 m respectively. On the contrary, Killari earthquake (1993/09/29,
559 Mw 6.5) showed lesser displacement (i.e. 0,5 m).
560 About this fundamental point, it is worthy to note that until now no coseismic ruptures (i.e.
561 surface faulting) were certainly reported even for the 1976 May 6th Friuli earthquake (Mw:6.5).
562 Cavallin et al. (1977), Bosi et al. (1976) and CNEN-ENEL Commission (1976) punctually
563 described diffuse geological effects of this earthquake as main ground cracks and sand mounds
564 in the epicentral area. In particular, Bosi et al. (1976) referred the ground crakes observed on the
565 Cuarnan Mt. to surficial expressions of deep dislocation linked to the May 6th earthquake.
566 Zanferrari et al., (2013) ruled out this possibility because of in correspondence of the major
567 ground crakes of Cuarnan Mt. no fault exists. The question why the May 6th Friuli earthquake
568 apparently did not generate coseismic surface faulting, remain at this time unsolved.
569 The only possible coseismic ruptures (about 18 cm of vertical displacement) were pinpointed by
570 Talamo (1977) between Venzone and Carnia localities (about 10 km northward Gemona del
571 Friuli) and later discussed by Pondrelli et al. (2001); Cheloni et al. (2012 and 2014). Poli and
572 Zanferrari (2018) ascribe this dislocation to the activation of the western segment of the Idrija
573 strike-slip fault (Idrija-Ampezzo strike slip fault in Zanferrari et al., 2013) during the seismic
574 sequence of September 1976 (Mw 6.1 and Mw 5.9).
575 The identification and the parametrization of active and capable faults at the front of the eastern
576 Southern Alps, characterized by compressive regime with low strain rate, considerably improve
577 the seismotectonic knowledge of the Veneto and Friuli regions and open new horizons for the
578 study of fault capability in very populated areas, such as NE Italy. Our results provide new data
579 to be incorporated in updated seismic hazards assessments for north-eastern Italy.

Acknowledgments

The research developed in the framework of the agreement between the Regione Autonoma Friuli Venezia Giulia - Direzione Centrale Ambiente ed Energia - Servizio Geologico, the Istituto Superiore per la Protezione e la Ricerca Ambientale (I.S.P.R.A.) and the University of Udine. The project was funded by the Regione Autonoma Friuli Venezia Giulia, Direzione Centrale Ambiente ed Energia, Servizio Geologico (C.I.G.: Z0E0C5EF75, p.i. Maria Eliana Poli). We are grateful to the Regione Autonoma Friuli Venezia Giulia – Direzione Centrale Ambiente ed Energia - Servizio Geologico for the permission to utilise and publish the collected environmental data. We are grateful to ENI s.p.a., Exploration & Production Division for the permission to study and publish seismic lines. Many thanks to Franz Livio, Riccardo Caputo, Dario Zampieri and an anonymous referee for the critical reviews that strongly improved the quality of the original manuscript.

We would like to thank Mrs. Emilia Del Bianco and Ing. Pietro Cassan for their support and assistance during trenching activities. Many thanks to Daniel Nieto for helping during the ERT and Seismic surveys.

Author contributions

MEP performed geological, morphological and structural analysis in collaboration with AZ and GM and interpreted the reflection seismic lines, writing the manuscript. EFa and SG led the paleoseismological investigations and wrote the relative chapter. The above authors contributed to the trenching activity, discussed the paleoseismological data and the general aspects concerning the regional seismotectonic framework.

AA, LB and GB achieved the SR and ERT survey; IDB and EFo carried out the GPR survey;

EDP and SG achieved the HVSR-MASW-ReMi combined survey; AM set up the artwork.

All the authors revised the manuscript.

Declaration of interests

The authors declare that they have no known competing financial interests or personal relationships that could have appeared to influence the work reported in this paper.

REFERENCES

Anderlini, L., Serpelloni, E., Tolomei, C., De Martini, P.M., Pezzo, G., Gualandi, A., Spada, G., 2020. New insights into active tectonics and seismogenic potential of the Italian Southern Alps from vertical geodetic velocities. Solid Earth, 11, 1681–1698, 2020. https://doi.org/10.5194/se-11-1681-2020, © Author(s) 2020.

Atanackov, J., Jamšek Rupnik, P., Jež, J., Celarc, B., Novak, M., Milanič, B., Markelj, A., Bavec, M., Kastelic, V., 2021. Database of Active Faults in Slovenia: Compiling a New Active Fault Database at the Junction Between the Alps, the Dinarides and the Pannonian Basin Tectonic Domains. Front. Earth Sci. 9:604388. doi: 10.3389/feart.2021.604388

Aoudia, A., Saraò, A., Bukchin, B., Suhadolc, P., 2000. The 1976 Friuli (NE Italy) thrust faulting earthquake: a reappraisal 23 years later. Geoph. Res. Lett. 27, 573-576.

Avigliano, R., Calderoni, G., Monegato, G., Mozzi, P., 2002a. The late Pleistocene–Holocene evolution of the Cellina and Meduna alluvial fans (Friuli NE Italy). Memorie Società Geologica Italiana 57, 133– 139.

Avigliano R., Monegato G., Zanolla S., Michelutti G., Mozzi P. 2002b. Comparison between geological and pedological records in the Cellina alluvial fan (Friuli, Italy). Il Quaternario – Italian Journal of Quaternary Science 15, 99-104.

Bajc, J., Aoudia, A., Saraò, A., Suhadolc, P., 2001. The 1998 Bovec-Krn mountain (Slovenia) earthquake sequence. Geophys. Res. Let. 28 (9), 1839-1842.

Barba, S., Finocchio, D., Sikdar, E., Burrato, P., 2013. Modeling the interseismic deformation of a thrust system: seismogenic potential of the Southern Alps. Terra Nova 25/3, 221–227.

Barbano, M.S., 1993. Reasseng intensity of some Friuli earthquakes at the turn of the Eighteen centuries. Terra Nova 5, 467-474.

Beauprêtre, S., Garambois, S., Manighetti, I., Malavieille, J., Sénéchal, G., Chatton, M., Davies, T., Larroque, C., Rousset, D., Cotte, N., Romano, C., 2012. Finding the buried record of past

earthquakes with GPR-based palaeoseismology: a case study on the Hope fault, New Zealand, Geophysical Journal International 189 (1), 73-100.

Bechtold, M., Battaglia, M., Tanner, D.C., Zuliani, D., 2009. Constrains on the active tectonics of the Friuli/NW Slovenia area from CGPS measurements and three-dimensional kinematic modelling. Journal of Geophysical Research 114, B033408, doi: 10.1029/2008JB005638.

Bernardis, G., Cecotti, C., Poli, M.E., Renner, G., Snidarcig, A., Zanferrari, A., 1996. Considerazioni sulla sismicità dell'area di Claut (Prealpi carniche) e sui danni causati dal terremoto del 13 aprile 1996. Atti del Convegno: "La Scienza e i terremoti: analisi e prospettive dall'esperienza del Friuli", Udine 14-15 novembre 1996. 61-68, Forum Editrice.

Bernardis, G., Poli, M.E., Snidarcig, A., Zanferrari, A., 2000. Seismotectonic and macroseismic characteristics of the earthquake of Bovec (NW Slovenia: April 12th 1998). Bollettino di Geofisica Teorica e Applicata 41 (2), 133-148.

Böhm, G., Brauchler, R., Nieto, D.Y., Baradello, L., Affatato, A., Sauter, M., 2013. A field assessment of site-specific correlations between hydraulic and geophysical parameters. Near Surface Geophysics 11, 473-483. doi:10.3997/1873-0604.2013034.

Boncio, P., Liberi, F., Caldarella, M., and Nurminen, F.-C., 2018. Width of surface rupture zone for thrust earthquakes: implications for earthquake fault zoning, Nat. Hazards Earth Syst. Sci., 18, 241–256, https://doi.org/10.5194/nhess-18-241-2018, 2018.

Bosi, C., Camponeschi, B., Giglio, G., 1976. Indizi di possibili movimenti lungo faglie in occasione del terremoto del Friuli del 6 maggio 1976. Boll. Soc. Geol. Ital., 95, 803-830.

Bressan, G., Bragato, P.L., 2009. Seismic deformation pattern in the Friuli-Venezia Giulia region (north-eastern Italy) and western Slovenia. Bollettino di Geofisica Teorica ed Applicata 50 (3), pp. 255-275.

Burrato, P., Poli, M.E., Vannoli, P., Zanferrari, A., Basili, R., Galadini, F., 2008. Sources of Mw 5+ earthquakes in northeastern Italy and western Slovenia: An updated view based on geological and seismological evidence. Tectonophysics 453, 157–176.

Caputo, R., 1993. Morphogenic earthquakes: a proposal. Bull. INQUA, Neotectonics Commission 16, 24.

Caputo, R., 2005. Ground effects of large morphogenic earthquakes. J. of Geodyn. 40 (2-3), 113-118.

Caputo, R., Poli, M.E., Zanferrari, A., 2010. Neogene-Quaternary tectonic stratigraphy of the eastern Southern Alps, NE Italy. Journal of Structural Geology 32, 1009-1027.

Carniel, R., Malisan, P., Barazza, F., Grimaz, S., 2008. Improvement of HVSR technique by wavelet analysis. Soil Dynamics and Earthquake Engineering 28(4), 321–327.

Carulli, G.B., Cozzi, A., Longo Salvador, G., Pernarcic, E., Podda, F., Ponton, M., 2000. Carta Geologica delle Prealpi Carniche. Pubbl. n° 44, Edizioni Museo Friulano Storia Naturale, Udine.

Castellarin, A., Cantelli, L., 2000. Neo-Alpine evolution of the Southern Eastern Alps. J. Geodyn. 30, 251-274.

Castellarin, A., Cantelli, L., Fesce, A.M., Mercier, J.L., Picotti, V., Pini, G.A., Prosser, G., Selli, L. 1992. Alpine compressional tectonics in the Southern Alps. Relationships with the N-Apennines. Annales Tectonicae 6, 62-94.

Cati, A., Fichera, R., Cappelli V.; 1989. Northeastern Italy. Integrated processing of geophysical and geological data. Mem. Soc. Geol. It., **40**, 273-288.

Cavallin, A., Martinis, B., Sfondrini, G., 1977. Effetti geologici del terremoto: fenditure nel terreno e "vulcanelli" di sabbia. In "Studio geologico dell'area maggiormente colpita dal terremoto friulano del 1976. A cura di Martinis B. Riv. Ital. Paleont. 83, 199-393.

Cheloni D., D'Agostino N., D'Anastasio E. Selvaggi G., 2012. Reassessment of the source of the 1976 Friuli, NE Italy, earthquake sequence from the joint inversion of high-precision levelling and triangulation data. Geophys. J. Int. 190, 1279–1294, doi: 10.1111/j.1365-246X.2012.05561.x

714 Cheloni, D., D'Agostino, N., Selvaggi, G., 2014. Interseismic coupling, seismic potential and
715 earthquake recurrence on the southern front of the Eastern Alps (NE Italy), J. Geophys. Res.
716 Solid Earth 119, 4448–4468, doi:10.1002/2014JB010954.
717
718 Commissione CNEN-ENEL, 1976. Contributo allo studio del terremoto del Friuli del maggio del
719 1976. 135 pag. 129 figs. Roma.
720
721 Cunningham, D., Gosar, A., Kastelic, V., Grebby, S., Tansey, K., 2007. Multi-disciplinary
722 investigations of active faults in the Julian Alps, Slovenia, Acta Geodyn. Geomater., 4(1), 77-85.
723
724 Dal Bo, I., 2015. Studio geofisico integrato di strutture tettoniche superficiali mediante tecniche
725 ad altissima risoluzione. Tesi inedita di Laurea Magistrale in Geoscienze. Università di Trieste,
726 119 pp. In Italian.
727
728 DISS Working Group, 2018. Database of Individual Seismogenic Sources (DISS), Version 3.2.1:
729 A compilation of potential sources for earthquakes larger than M 5.5 in Italy and surrounding
730 areas. http://diss.rm.ingv.it/diss/, Istituto Nazionale di Geofisica e Vulcanologia;
731 DOI:10.6092/INGV.IT-DISS3.2.1.
732
733 Doglioni, C., 1992. The Venetian Alps thrust belt. In: McKlay K.R. (Ed.), Thrust Tectonics, 319-
734 324, Chapman and Hall, London.
735
736 Doglioni, C., Bosellini, A., 1987. Eoalpine and mesoalpine tectonics in the Southern Alps. Geol.
737 Rundsch. 76, 735-754.
738
739 Ercoli, M., Pauselli, C., Frigeri, A., Forte, E., Costanzo, F., 2014. 3-D GPR data analysis for
740 high-resolution imaging of shallow subsurface faults: the Mt. Vettore case study (Central
741 Apennines, Italy), Geophysical Journal International 198(1), 609–621.
742
743 Ercoli, M., Pauselli, C., Cinti, F., Forte, E., Volpe, R., 2015. 3D active fault imaging: comparison
744 between outcrops and GPR data. The example of the Castrovillari fault (Calabria, southern
745 Italy), Interpretation 3 (3), pp. SY57-SY66. doi 10.1190/INT-2014-0234.1.
746
747 Falcucci, E., Poli, M.E., Galadini, F., Scardia, G., Paiero, G., Zanferrari A., 2018. First evidence
748 of active transpressive surface faulting at the front of the eastern Southern Alps, northeastern

Italy: insight on the 1511 earthquake seismotectonics. Solid Earth, 9, 911-922, https://doi.org/10.5194/se-9-911-2018,2018.

Fantoni, R., Catellani, D., Merlini, S., Rogledi, S., Venturini, S., 2002. La registrazione degli eventi deformativi cenozoici nell'avampaese Veneto-Friulano. Mem. Soc. Geol. It. 57, 301-313.

Feruglio, E., 1929. Nuove ricerche sul Quaternario del Friuli. Giornale di Geologia 4, 1–36.

Galadini, F., Poli, M.E., Zanferrari, A., 2005. Seismogenic sources potentially responsible for earthquakes with M ≥ 6 in the eastern Southern Alps (Thiene-Udine sector, NE Italy). Geophys. J. Int. 161, 739-762. doi: 10.1111/j.1365-246X.2005.02571.x.

Grimaz, S., Malisan, P., Barazza, F., Carniel, R., 2014. Rapid instrumental check of vulnerability parameters on bridges for seismic risk mitigation purposes. Bollettino di Geofisica Teorica ed Applicata 54 (3), 205–215.

Kastelic, V., Vrabec, M., Cunningam, D., Gosar, A., 2008. Neoalpine structural evolution and present day tectonic activity of the eastern Southern Alps: the case of the Ravne fault, NW Slovenia. J. Structural Geol. 30, 963-965.

Lambeck, K., Rouby, H., Purcell, A., Sun, Y., Sambridge, M., 2014. Sea level and global ice volumes from the Last Glacial Maximum to the Holocene. PNAS 111, 15296–15303.

Livio F., Kettermannb, M., Reicherterc, K., Uraib J. L., (2019). Growth of bending-moment faults due to progressive folding: Insights from sandbox models and paleoseismological implications. Geomorphology 326, 152-166.

Loke, M.H., Barker, R.D., 1996. Rapid least-squares inversion of apparent resistivity pseudosections by a quasi-Newton method. Geophysical Prospecting 44, 131-152.

Louie, J. N., 2001. Faster, better shear-wave velocity to 100 meters depth from refraction microtremor arrays. Bulletin of the Seismological Society of America 91 (2), 347-364.

Massari, F., Grandesso, P., Stefani, C., Zanferrari, A., 1986. The Oligo-Miocene Molasse of the Veneto-Friuli region, Southern Alps. Giorn. Geol. 48, 235-255.

McCalpin, J., 2009. Paleoseismology, 2nd edition. Academic Press, an imprint of Elsevier, Amsterdam. (848 pp.).

McClymont, A.F., Green, A.G., Streich, R., Horstmeyer, H., Tronicke, J., Nobes, D.C., Pettinga, J., Campbell, J., Langridge, R., 2008. Visualisation of active faults using geometric attributes of 3D GPR data: an example from the Alpine Fault Zone, New Zealand. Geophysics 73 (2), B11–B23.

Meroni, F., Pessina V., Bernardini A., 2008. Damage risk and scenarios in the Veneto - Friuli area (NE Italy). Boll. Geof. Teor. Appl. 49, n.3-4, 485-504.

Monegato, G., Lowick, S. E., Ravazzi, C., Banino, R., Donegana, M. and Preusser, F. 2009. Middle to Late Pleistocene palaeoenvironmental evolution of the southeastern Alpine Valeriano Creek succession (northeastern Italy). J. Quaternary Sci., Vol. 25 pp. 617–632. ISSN 0267-8179.

Monegato, G., Stefani, C., Zattin, M., 2010. From present rivers to old terrigenous sediments: the evolution of the drainage system in the eastern Southern Alps. Terra Nova 22, 218–226.

Monegato, G., Poli, M.E., 2015. Tectonic and climatic inferences from the terrace staircase in the Meduna valley, eastern Southern Alps, NE Italy. Quaternary Research 83, 229-242.

Monegato, G., Ravazzi, C., 2018. The Late Pleistocene multifold glaciation in the Alps: updates and open questions. Alpine and Mediterranean Quaternary, 31, 225-229.

Moulin, A., Benedetti, L., Gosar, A., Rupnik, P. J., Rizza, M., Bourlès, D., Ritz, J. F., 2014. Determining the present-day kinematics of the Idrija fault (Slovenia) from airborne LiDAR topography, Tectonophysics 628, 188–205.

Nurminen, F., Boncio, P., Visini, F., Pace, B., Valentini, A., Baize, S., Scotti, O., 2020. Probability of Occurrence and Displacement Regression of Distributed Surface Rupturing for Reverse Earthquakes. Front. Earth Sci. 8:581605. doi: 10.3389/feart.2020.581605.

817 Paiero, G., Monegato, G., 2003. The Pleistocene evolution of Arzino alluvial fan and western
818 part of Tagliamento morainic amphitheatre (Friuli, NE Italy). Il Quaternario–Italian Journal of
819 Quaternary Sciences 16 (1), 185–193.
820
821 Park, C.B., Miller, R.D., Xia, J. (1999). Multichannel analysis of surface waves. Geophysics,
822 64(3), 800-808.
823
824 Patricelli, G., Poli, M.E., 2020. Quaternary tectonic activity in the North-eastern Friuli Plain (NE
825 Italy). Bollettino di Geofisica Teorica ed Applicata 61/3, 309-332. DOI 10.4430/bgta0319.
826
827 Peruzza, L., Poli, M.E., Rebez, A., Renner, G., Rogledi, S., Slejko, D., Zanferrari, A., 2002. The
828 1976-1977 seismic sequence in Friuli: new seismotectonic aspects. Mem. Soc. Geol. It. 57, 391-
829 400.
830
831 Poli, M.E., Renner, G., 2004. Normal focal mechanisms in the Julian Alps and Prealps:
832 seismotectonic implications for the Italian-Slovenian border region. Boll. Geof. Teor. Appl. 45,
833 51-69.
834
835 Poli, M.E., Zanferrari, A., 2018. The seismogenic sources of the 1976 Friuli earthquakes: a new
836 seismotectonic model for the Friuli area. Boll. Geof. Teor. Appl. 59(4), 463-488.
837
838 Poli, M.E., Zanferrari, A., Monegato, G., 2009. Geometria, cinematica e attività pliocenico-
839 quaternaria del sistema di sovrascorrimenti Arba-Ragogna (Alpi Meridionali orientali, Italia
840 NE). Rendiconti online Società Geologica Italiana 5, 172-175.
841
842 Poli, M.E., Monegato, G., Zanferrari, A., Falcucci, E., Marchesini, A., Grimaz, S., Malisan, P.,
843 Del Pin, E. 2015. D6/a2.1 - Seismotectonic characterization of the western Carnic pre-alpine area
844 between Caneva and Meduno (NE Italy, Friuli). In "Base-knowledge improvement for assessing
845 the seismogenic potential of Italy". DPC-INGV-S1 Project 2014-15 – Internal report, 22 pp.
846
847 Poljak, M., Zivcic, M., Zupančič, P., 2000. The seismotectonic characteristics of Slovenia. Pure
848 Appl. Geophys. 157, 37–55.
849
850 Pondrelli, S., Ekström, G., Morelli, A. 2001. Seismotectonic re-evaluation of the 1976 Friuli,
851 Italy, seismic sequence. Journal of Seismology 5, 73-83.

Ponton, M., 2010. Architettura delle Alpi Friulane. Museo Friulano Storia Naturale, pubbl. 52, 80 pp.

Reimer, P., Bard, E., Bayliss, A., Beck, J., Blackwell, P., Ramsey, C., . . . Van der Plicht, J. (2013). IntCal13 and Marine13 Radiocarbon Age Calibration Curves 0–50,000 Years cal BP. *Radiocarbon, 55*(4), 1869-1887. doi:10.2458/azu_js_rc.55.16947

Rovida A., Locati M., Camassi R., Lolli B., Gasperini P., Antonucci A. (2021). Catalogo Parametrico dei Terremoti Italiani (CPTI15), versione 3.0. Istituto Nazionale di Geofisica e Vulcanologia (INGV). https://doi.org/10.13127/CPTI/CPTI15.3

Schönborn, G., 1999. Balancing cross sections with kinematic constrains the Dolomites (norther Italy). Tectonics 18 (3), 527-545.

Serpelloni, E., Vannucci, G, Anderlini, L., Bennett, R.A., 2016. Kinematics, seismotectonics and seismic potential of the eastern sector of the European Alps from GPS and seismic deformation data. Tectonophysics 688, 157–181.

SESAME, 2004. Guidelines for the implementation of the H/V spectral ratio technique on ambient vibrations: measurements, processing and interpretation. SESAME European research project EVG1-CT-2000-00026, deliverable D23.12.

Stefani, C., 1982. Geologia dei dintorni di Fanna e Cavasso Nuovo (Prealpi Carniche). Mem. Sci. Geol., **35**: 203-212, Padova.

Stewart, R., 1993. Exploration Seismic Tomography: Fundamentals. vol. 3 of Course Note Series, Society of Exploration Geophysicists. doi: 10.1190/1.9781560802372.

Talamo, R., Pampaloni, M., Grassi, S., 1978. Risultati delle misure di livellazione di alta precisione eseguite dall'Istituto Geografico Militare nelle zone del Friuli interessate dalle recenti attività sismiche. Boll. Geod. Sc. Aff., **1**, 6-75.

Toscani, G., Marchesini, A., Barbieri, C., Di Giulio, A., Fantoni, R., Mancin, N., Zanferrari, A., 2016. The Friulian-Venetian Basin I: architecture and sediment flux into a shared foreland basin. Ital. J. Geosci. 135 (3), 444-459. (doi: 10.3301/IJG.2015.35).

Venturini, C., Discienza, K., Astori, A., 2013. Sedimentologia e tettonica della successione clastica della Val Meduna (Prealpi Carniche, PN). Gortania, Atti Museo Friulano di Storia Naturale 34 (2012), 51–78.

Vesnaver, A., Böhm, G., 2000. Staggered or adapted grids for seismic tomography? The Leading Edge 9, 944-950. doi: 10.1190/1.1438762.

Vrabec, M., Fodor, L. 2006. Late Cenozoic tectonics of Slovenia: structural styles at the Northeastern corner of the Adriatic microplate. In: Pinter, N., Grenerczy, G., Weber, J., Stein, S., Medak, D. (Eds.). The Adria Microplate: GPS Geodesy, Tectonics and Hazards. Nato Science Series IV: Earth and Environmental Sciences, 61, Springer, pp. 151-168.

Wells, D.L., Coppersmith, K.J. 1994. New empirical relationships among magnitude, rupture length, rupture width, rupture area, and surface displacement. Bull. Seism. Soc. Am. 84 (4), 974-1002.

Zanferrari, A., Avigliano, R., Monegato, G., Paiero, G., Poli, M.E., Stefani, C., 2008a. Geological map and explanatory notes of the Geological Map of Italy at the scale 1:50.000: Sheet 066 “Udine”. APAT-Servizio Geologico d’Italia – Regione Autonoma Friuli Venezia Giulia, 176 pp. http://www.isprambiente.gov.it/Media/carg/friuli.htm.

Zanferrari, A., Avigliano, R., Grandesso, P., Monegato, G., Paiero, G., Poli, M.E., Stefani, C., 2008b. Geological map and explanatory notes of the Italian Geological Map at the scale 1:50.000: Sheet 065 “Maniago”. APAT-Servizio Geologico d’Italia – Regione Autonoma Friuli Venezia Giulia. http://www.isprambiente.gov.it/Media/carg/friuli.html.

Zanferrari, A., Masetti, D., Monegato, G., Poli, M.E., 2013. Geological map and explanatory notes of the Geological Map of Italy at the scale 1:50.000: Sheet 049 “Gemona del Friuli”. ISPRA - Servizio Geologico d’Italia - Regione Autonoma Friuli Venezia Giulia, 262 pp. http://www.isprambiente.gov.it/Media/carg/friuli.html.

Zattin, M., Stefani, C., Martin, S., 2003. Detrital fission-track analysis and sedimentary petrofacies as keys of Alpine exhumation; the example of the Venetian foreland (European Southern Alps, Italy). J. Sediment. Res. 73, 1051–1061. doi:10.1306/051403731051.

LIST OF TABLES

CAPTION FIGURES

Figure 1. Tectonic sketch map of the eastern Southern Alps in NE-Italy and W-Slovenia (modified from Zanferrari et al., 2013). Red stars: historical and instrumental seismicity (Mw>5.5, according DBMI 2015). Red rectangle: the study area of Fig. 2. Legend: AR: Arba-Ragogna Thrust; BV: Bassano–Vittorio Veneto Th.; BFC: Borgo Faris–Cividale Fault; CA: Cansiglio Th.; FS: Fella–Sava Fault; GK: Gemona–Kobarid Th.; HS: Hochstuhl Fault; IA: Idrija–Ampezzo Fault; MC: Mt. Ciaurlec Th.; MD: Medea Th.; MJTS: Mt. Jouf Thrust-System; MT: Montello Th.; PA: Palmanova Th.; PE: Periadriatic Th.; PL: Periadriatic Lineament; PM: Polcenigo-Montereale Th.; PR: Predijama Fault; PZ: Pozzuolo Th.; RA: Resiutta-Ponte Avons Fault; RP: Ravne–Paularo Fault; RS: Raša Fault; ST: Susans-Tricesimo Th.; UB: Udine–Buttrio Th.; VB: Valsugana-Val Bordaglia Th.

Figure 2. Geological sketch map of the pre-alpine area between Cellina and Cosa Rivers (modified from Carulli et al., 2000; Zanferrari et al, 2008b; Monegato and Poli, 2015 and Poli et

al., 2015). Shaded relief from DTM supplied by Friuli Venezia Giulia Region (grid: 10x10m). Legend: AR: Arba–Ragogna Thrust; DT: Duranno–Tramonti Th.; ML: Maniago Libero Th.; MC: Monte Ciaurlec Th.; ME: Meduno Th.; ME_1: Meduno 1 external splay of Meduno Th.(see Fig. 5); MJ: Mt. Jouf Th.; PI: Pinzano Th.; PM: Polcenigo – Montereale Th.; PE: Periadriatic Th.; SE: Sequals Th.; SI: Silisia Th.; SO: Solimbergo Th; TO: Toppo Tear Fault; TV: Travesio Th. Near Meduno locality, the Rivalunga terrace (R. t.).

Figure 3. Geological section HH' (location in Fig. 2). Source data: for the piedmont plain Zanferrari et al., (2008b) and seismic lines gently supplied by ENI, Exploration & Production Division. For the relief: original geological survey and Carulli et al. (2000). PT: Permian-Middle Triassic undifferentiated succession (from Cati et al., 1987); C.u.: Carnian unconformity (Travenanzes Formation); DPR: Upper Triassic carbonate platforms; FCP: undifferentiated Lower Jurassic-Upper Cretaceous carbonate platforms; FLY: Lower Eocene emipelagic and turbiditic successions (Scaglia Rossa Friulana and Clauzetto Flysch); CAV: Aquitanian–Lower Serravallian Cavanella Group; AT: Lower Serravalian–Tortonian (Marna di Tarzo and Arenaria di Vittorio Veneto fms.); MON1+2: Upper Tortonian–Lower Messinian Montello Conglomerate members; MON3: Lower Messinian Montello Conglomerate member; FS: pre-LGM Pliocene-Quaternary continental succession (Friuli Supersynthem); UPH: Upper Pleistocene (LGM) – Holocene pp. alluvial and fluvioglacial deposits of the Meduna catchment. Present alluvial deposits were not mapped. Capped lines: W-verging Paleogene Dinaric Mt. Ciaurlec Thrust.

Figure 4. Progressive deformation involving the Pliocene(?) Del Bianco Conglomerate along the high angle, S-SE verging Monte Jouf reverse fault near Valle locality (location in Fig. 2).

Figure 5. The base of the Pliocene(?)– Quaternary succession (green line) is cut and displaced $Meduno_1$ Th. (i.e. ME_1 in Fig. 2). Legend: PQ: Pliocene-Quaternary succession; SM: Serravallian – Messinian Southalpine Molasse; KK' trace of the seismic profile in Fig. 2. Seismic line (excerpt) gently supplied by Eni Exploration & Production Division.

Figure 6. **a**) Left side of River Meduna near Ponte Maraldi (Meduno). For location, see Fig. 2 and Fig. 7. The overturned Upper Miocene Montello Conglomerate (UM: blue dotted line) and the sub-horizontal PRELGM and LGM gravels of the Meduna River (LGM bottom: yellow line) join along the high-angle, NNE-SSW striking, WNW-dipping oblique ramp of the Meduno Thrust. Along the fault surface, gravels are fractured, rotated and dragged (**b**). **c**) Deformed Miocene conglomerates (Montello Fm.) outcropping in the riverbed of the Meduna River in front of the Ponte Maraldi. Topographic surface (black traced lines) and elevations from CTRN 048140-Meduno.

Figure 7. Geological and geomorphological map of the study area (location in Fig. 2). Shaded relief from DTM supplied by Friuli Venezia Giulia Region (grid: 1x1m). Red line: Meduno Thrust as observed in the paleoseismological trenches and around Ponte Maraldi. Brown lines: S1-line, S2-line, S3-line and S4-line (i.e. traces of seismic reflection, seismic tomography and geoelectrical profiles of Figs: 8, 9, 10 and 11); AA', BB', CC' and DD': geological cross sections of Figs. 8d, 9d, 10d and 11d respectively. Yellow lines: GPR profiles of Figs. 14 and 15. Light green areas: paleoseismological trenches MED_EAST and MED_WEST. White asterisk marks Ponte Maraldi location (Fig. 5). CAV: Aquitanian–Lower Serravallian Cavanella Group; AT: Lower Serravallian–Tortonian (Marna di Tarzo and Arenaria di Vittorio Veneto Fms.); MON: Upper Tortonian–Lower Messinian Montello Conglomerate; PRELGM: Pliocene-Quaternary continental succession (Friuli Supersynthem); UPH: Upper Pleistocene (LGM) – Holocene pp. alluvial and fluvioglacial deposits of the Meduna catchment; HOL: Present alluvial deposits.

Figure 8. Geophysical interpretation of the S2-line (location in Fig. 7). **a**) Seismic reflection stack does not show any tectonic disturbance. Yellow line: top of the Upper Miocene Molasse. Blue areas indicate not reliable seismic data; **b**) Seismic tomography identifies three sub-horizontal seismo-stratigraphic layers (blue dotted lines), confirming the un-deformed setting of the sedimentary succession. **c**) Along the ERT section, no abrupt resistivity contact was observed. Low resistivity values correspond to local springs. **d**) Geological cross section (BB' in fig. 7) shows a regular stratigraphic setting. Legend: MON: Upper Tortonian–Lower Messinian Montello Conglomerate; PRELGM: Pliocene-Quaternary continental succession (Friuli Supersynthem); UPH: Upper Pleistocene (LGM) – Holocene pp. alluvial and fluvioglacial deposits of the Meduna catchment.

Figure 9. Geophysical and geological interpretations of the S1 line (location in Fig. 7). **a**) Seismic reflection stack: in correspondence of the tectonic scarp a complex transpressive high angle, tectonic system (red lines) displaces the erosive boundary between the PRELGM deposits and the Upper Miocene Molasse (yellow line) and involves the Quaternary succession. Blue areas: not reliable seismic data. **b**) Seismic tomography: red lines pinpoint the anomalous velocity distribution across the tectonic scarp. Blue dotted lines: bedding of the main sedimentary bodies. In the western edge, note the high velocity body corresponding to the Montello conglomerate that crops out along the left side of the Meduna River. **c**) Electrical resistivity tomography confirms an abrupt change in resistivity values along the tectonic scarp (black arrow)**. d**) Geological interpretation (AA' in Fig. 7) based on the geophysical data and the geological survey along the left side of the Meduna River. Legend: AT: Lower Serravallian–Tortonian (Marna di Tarzo and Arenaria di Vittorio Veneto Fms.); MON: Upper Tortonian–Lower Messinian Montello Conglomerate; PRELGM: Pliocene-Quaternary continental succession (Friuli Supersynthem); UPH: Upper Pleistocene (LGM) – Holocene pp. alluvial and fluvioglacial deposits of the Meduna catchment; HOL: Present alluvial deposits of the Meduna River.

Figure 10. Geophysical interpretation of the S3 line (location in Fig. 7). **a**) Seismic reflection stack: a complex transpressive structure (red lines) develops across the tectonic scarp in the western sector of the section and strongly involves the Quaternary succession. Yellow line: erosive boundary between the pre-LGM deposits and the Upper Miocene Molasse. Note that the most surficial seismic horizon (probably corresponding to the Unit 1 of the MEDU_WEST) is cut off by the transpressive fault just upstream of the paleoseismological trench. Blue areas not reliable seismic data. **b**) Seismic tomography shows abrupt changes in the velocity in the western portion. Blu lines: bedding of the sedimentary bodies. **c**) Electrical resistivity tomography confirms an abrupt change in resistivity values along the tectonic scarp (black arrows). **d**) Geological interpretation (CC' in Fig. 7). Legend: AT: Lower Serravallian–Tortonian (Marna di Tarzo and Arenaria di Vittorio Veneto Fms.); MON: Upper Tortonian–Lower Messinian Montello Conglomerate; PRELGM: Pliocene-Quaternary continental succession (Friuli Supersynthem); UPH: Upper Pleistocene (LGM) – Holocene pp alluvial and fluvioglacial deposits of the Meduna catchment; HOL: Present alluvial deposits. Note that the Quaternary

succession strongly thickens toward the South crossing the tectonic scarp. MASW-V and MASW-M as in Fig. 12.

Figure 11. Geophysical interpretation of the S4-line (location in Fig. 7): **a**) seismic reflection stack shows a high angle S-verging reverse fault (red lines) crossing the tectonic scarp. Yellow line: erosive boundary between the Upper Miocene Molasse and the pre-LGM deposits. Blue areas not reliable seismic data. **b**) Seismic tomography shows an abrupt variation in the velocity in correspondence of the scarp (western portion). Blue lines: bedding of the sedimentary bodies. **c**) Electrical resistivity tomography confirms an abrupt change in resistivity values along the tectonic scarp of the Rivalunga terrace. **d**) Geological interpretation (DD' in Fig.7) of the geophysical data. Legend: AT: Lower Serravallian–Tortonian (Marna di Tarzo and Arenaria di Vittorio Veneto fms.); MON: Upper Tortonian–Lower Messinian Montello Conglomerate; PRELGM: Pliocene-Quaternary continental succession (Friuli Supersynthem); UPH: Upper Pleistocene (LGM) – Holocene p.p. alluvial and fluvioglacial deposits of the Meduna catchment.

Figure 12. Western edge of the Rivalunga terrace where passive seismic investigations (ReMI, MASW and HVSR: pink lines and pink points respectively) were carried out. Legend: AT: Lower Serravallian–Tortonian (Marna di Tarzo and Arenaria di Vittorio Veneto Fms.); MON: Upper Tortonian–Lower Messinian Montello Conglomerate; PRELGM: Pliocene-Quaternary continental succession (Friuli Supersynthem); UPH: Upper Pleistocene (LGM) – Holocene pp alluvial and fluvioglacial deposits of the Meduna catchment; HOL: Present alluvial deposits. More details in the text.

Figure 13. Data set of passive seismic investigations on the western edge of the Rivamonte terrace. **a**) Natural microtremor was recorded along two alignments of measurement points (HV1 and HV2). The major changes of natural frequency were identified close to the scarp, where interpretation of the HVSR data indicates a significant increase in thickness of the Quaternary stratigraphic layers (**b, c**). PRELGM: Pliocene-Quaternary continental succession (Friuli Supersynthem); UPH: Upper Pleistocene (LGM) – Holocene pp alluvial and fluvioglacial deposits of the Meduna catchment.

Figure 14. GPR profiles (GPR 3 and GPR 4 in Fig. 7) crossing the tectonic scarps in correspondence of the paleoseismological trenches. Red lines on the profiles mark the main lateral discontinuities, green lines refer to S-SE-dipping reflectors, orange lines reflector with opposite dip (N –NW), while pink lines highlight a shallow reflector sub parallel to the topographic surface.

Figure 15. Detail of profile GPR 4, collected in the zone of MED_EAST trench (Fig. 7). a) Reflection amplitude, b) cosine of instantaneous phase, c) dominant frequency, d) sweetness, e) chaos, f) trace gradient. Dashed red lines mark the most apparent lateral discontinuity. Main diffractions are marked by letter D. No vertical exaggeration. Please see text for description of horizons H0-H6.

Figure 16. Paleoseismological trench MED_WEST (**a**) and relative interpretation (**b**). Location in Fig. 7. Scarp on the right. One metre for the mesh grid. Note the thickening of Unit 3 toward the South and warping of the contact between Unit 3 and the underlying units in proximity of the scarp. Numbers refer to the stratigraphic units described in the text. Red lines: reverse faults; violet lines: normal extrados shear surfaces. (**c**) Stereographic projection of thrusts and fractures collected in the damage zone of MED_WEST. Black squares refer to dragging clasts collected on the reverse tectonic surfaces (i.e. maximum stretching of the clasts were considered as a lineation). **d**) Spatial relationship between the trench MED_WEST and the scarp: excavation did not affect the scarp, which was strong reworked by human activity.

Figure 17. Paleoseismological trench MED_EAST (**a, b, c**), particular of the shear zone affected unit 3 (**d**) and interpretation of trench wall (**e**). Location in Fig. 7. One metre for the mesh grid. Thickening of unit 3 toward the South and warping of the contact between unit 3 and the underlying units happens in proximity of the scarp (in the left). Numbers refer to the stratigraphic units in the text. Red lines: reverse faults. **f**) Spatial relationship between the trench MED_EAST and the scarp: excavation did not affect the scarp, which was strong reworked by human activity (see for example the dry stone-wall and the aligned trees).

Figure 18. MED_WEST: the damage zone localised near the tectonic scarp. The oldest event (E2; Fig. 18 **a, b, c**) displaced unit 5 on unit 4 along F1. The subsequent event (E1) involved also unit 3 along F2 shear zone (Fig. 18 **d, e, f**). One metre for the mesh grid.

Figure 19. (**a**) Extrados fractures at the northern portion of the trench MED_WEST (green rectangle in fig. 16) and relative interpretation (**b**). One metre for the mesh grid. The extrados features do not propagate in depth but end at roughly 3-4 m-depth, as visible in "c", which locates downward with respect to the central fractures. Picture in "c" shows the wall (oblique view with respect to main trench wall) of the small excavation dug at the base of the trench).

Figure 20. Structural setting of the study area and macroseismic damage distribution of the 1776 earthquake; red star and blue square: macroseismic epicentres (from DBMI, 2015).

Supplemetary Figure S1. Restoration of paleoseismological trench MED_WEST. Numbers refer to stratigraphic units described in the text. Dotted lines: erosional surfaces. Not to scale.

Supplementary Figure S2. Restoration of paleoseismological trench MED_EAST. Numbers refer to stratigraphic units described in the text. Dotted line: erosional surface. Not to scale.

Supplementary Figure S3. Seismic reflection stack (**a**), seismic tomography (**b**) and electrical resistivity tomography (**c**) of S1-line (location in Fig. 7). Not interpreted.

Supplementary Figure S4. Seismic reflection stack (**a**), seismic tomography (**b**) and electrical resistivity tomography (**c**) of S2-line (location in Fig. 7). Not interpreted.

Supplementary Figure S5. Seismic reflection stack (**a**), seismic tomography (**b**) and electrical resistivity tomography (**c**) of S3-line (location in Fig. 7). Not interpreted.

Supplementary Figure S6. Seismic reflection stack (**a**), seismic tomography (**b**) and electrical resistivity tomography (**c**) of S4-line (location in Fig. 7). Not interpreted.

Table 1 – Historical events with Mw≥5.5 in Carnic Prealps (Rovida et al., 2021). Epicentre locations in Fig. 1.

Year	Epicentre locality	Io (MCS)	Mw
1776/07/10	Prealpi friulane	8-9	5.8
1794/06/07	Prealpi friulane	8-9	5.9
1812/10/25	Pordenonese	7-8	5.6
1873/06/29	Alpago	9-10	6.3
1936/10/18	Cansiglio	9	6.0

Table 2: data acquisition system, parameters and processing steps used in this study.

Method	Acquisition apparatus	Acquisition parameters	Data processing
Electrical Resistivity Tomography (ERT)	Georesistivimeter LGM Lippmann (Schaufling-Germany) mod. 4-Punkt light10W. The system allows the possibility of using up to 255 electrodes – maximum distance of 5 meters. -Connector/Active electrodes: ActEle system. Geoelectrical data acquisition software: GeoTest	-electrode array: Dipole-Dipole -connector spacing: 2.50 m profile ERT-line 1, ERT-line 2, ERT-line 3. -connector spacing: 3 m profile ERT-line 4A, ERT-line 4B.	Inversion program: RES2DINV (Loke and Barker, 1996). The topographic correction was performed importing the GNSS data (Global Navigation Satellite System) acquired with a Topcon GR-5 Receiver and FC-500 Hand-held controller.
Seismic survey: Seismic refraction tomography (SRT) and Seismic reflection (SR)	DMT Summit II (24 bits) Source: Isotta seismic armed with industrial 8 cartridge (depth 0.3 m). Geophones resonance Frequency 10 Hz	- number of active channels from 101 to 343 (depend on profile length) - station interval 2 m - source interval 4 m - sampling interval 0.25 ms - recording time 1024 ms - pre trigger 10 ms	SR processing: 1) geometry and trace editing; 2) geometrical spreading recovery and gain (Inversion curve); 3) band-pass filtering; 4) static corrections from first breaks (CAT3D); 5) trimmed mean dynamic dip to remove ground roll; 6) sort semblance velocity analysis and corresponding normal move out; 7) Alpha-trim stacking. SRT procedure: 1) picking of the first arrivals; 2) travel time inversion of the first arrivals (CAT3D); 3) depth P-velocity models
HVSR combined with ReMi, MASW and seismic refraction	Lennartz M24 Compact/LP portable network seismograph (24 bits). Lennartz Le-3Dlite seismometers, 1 s. Geometrics Geode Exploration Seismograph (24 bits). 24 geophones with natural	- HVSR: acquisition time 20 min, sampling 125 Hz; - ReMi: geophones distance 2.5 and 5 m, sampling interval 2 ms, recording time 30 s; - MASW: geophones distance 2.5 and 5 m, sampling interval 2 ms, recording time 10 s, sources offset	HVSR processing: algorithms developed by SPRINT-Lab researchers (Carniel et al., 2008; Grimaz et al., 2013), which implemented SESAME guidelines (SESAME, 2004). ReMi and MASW processing: SeisOpt® ReMi™ (© Optim, Inc.). Seismic refraction processing: PickWin™.

	frequency of 4.5-Hz. Shot source: 5kg sledgehammer on metal plate; mini-bang.	5 m; - Seismic refraction: geophones distance 2.5 and 5 m, sampling interval 0.125 ms, different source positions aligned with the linear array.	
Ground Penetrating Radar (GPR)	ProEx Malå Geoscience (GuidelineGeo) Equipped with 250 MHz shielded antennas	512 samples per trace; sampling interval 0.399 ns, trace interval 0.05 m, vertical stacking 16; RTK GPS positioning.	Zero time correction; DC removal; background removal; bandpass filtering; exponential amplitude recovery; datuming and topographic correction; diffraction hyperbolas velocity analysis; depth conversion and migration; attribute analysis.

Table 3: Soil depth and velocity values along the M and V-profiles

M profile thickness (m)	M profile Vp (m/sec)	Geologic interpretation	V profile Vp (m/sec)	V profile thickness (m)
1-3	440	top-soil	460	1-3
3-8	930	LGM deposits	1050	3-20
8 -	1780	pre-LGM deposits	1800	20 -

Table 4 - Radiocarbon dating performed on the collected samples (calibration curve by Reimer et al., 2013).

Stratigraphic Unit (and related trench)	*Sample*	*Material*	*Conventional radiocarbon age (years BP)*	*d13D*	*Calibrated age (2sigma; IntCal13)*
Unit 3 (MED_EAST)	MEDU_EST_4	Charcoal	320 ± 30 BP	-25 ‰	1470–1650 AD
Unit 3 (MED_EAST)	MEDU_EST_10	Charcoal	320 ± 30 BP	-23.2 ‰	1470–1650 AD
Unit 3 (MED_EAST)	MEDU_EST_12	Charcoal	520 ± 30 BP	-24.1 ‰	1330–1440 AD
Unit 6 (MED_EAST)	MEDU_EST_8	Charcoal	35920 ± 280 BP	-28.5 ‰	39225–37995 BC
Unit 3 (MED_WEST)	MEDU_OVEST_bulk_2	Bulk	2370 ± 30 BP	-24.1 ‰	510–395 BC

Table 5 – Geometric and kinematic parameters of the Meduno Thrust

Geometric and kinematic parameters	*Meduno Thrust*
Max surface length	8 km
Max depth (supposed)	6-8 km
Dip direction and dip of the fault plane	N 330°/45°- N 280°/70° - N330°/45°
Rake	90° - 60°
LGM – Present vertical slip	0.6 mm/yr (Monegato and Poli, 2015)
Latest observed displacement at the surface	20 cm on historical deposits (unit 2);
Max Mw from Wells and Coppersmith, (1994).	5.9 - (Ruptured area on reverse fault) 5.8 – (Subsurface rupture length on reverse fault) 5.8 – (Maximum Displacement: 0,20 m)
Latest earthquake	1776.07.10 (Mw: 5.8; Io 8-9) from DBMI15

Figure 1

Click here to access/download;Figure (with caption below and on the same page);Figure 1.tif

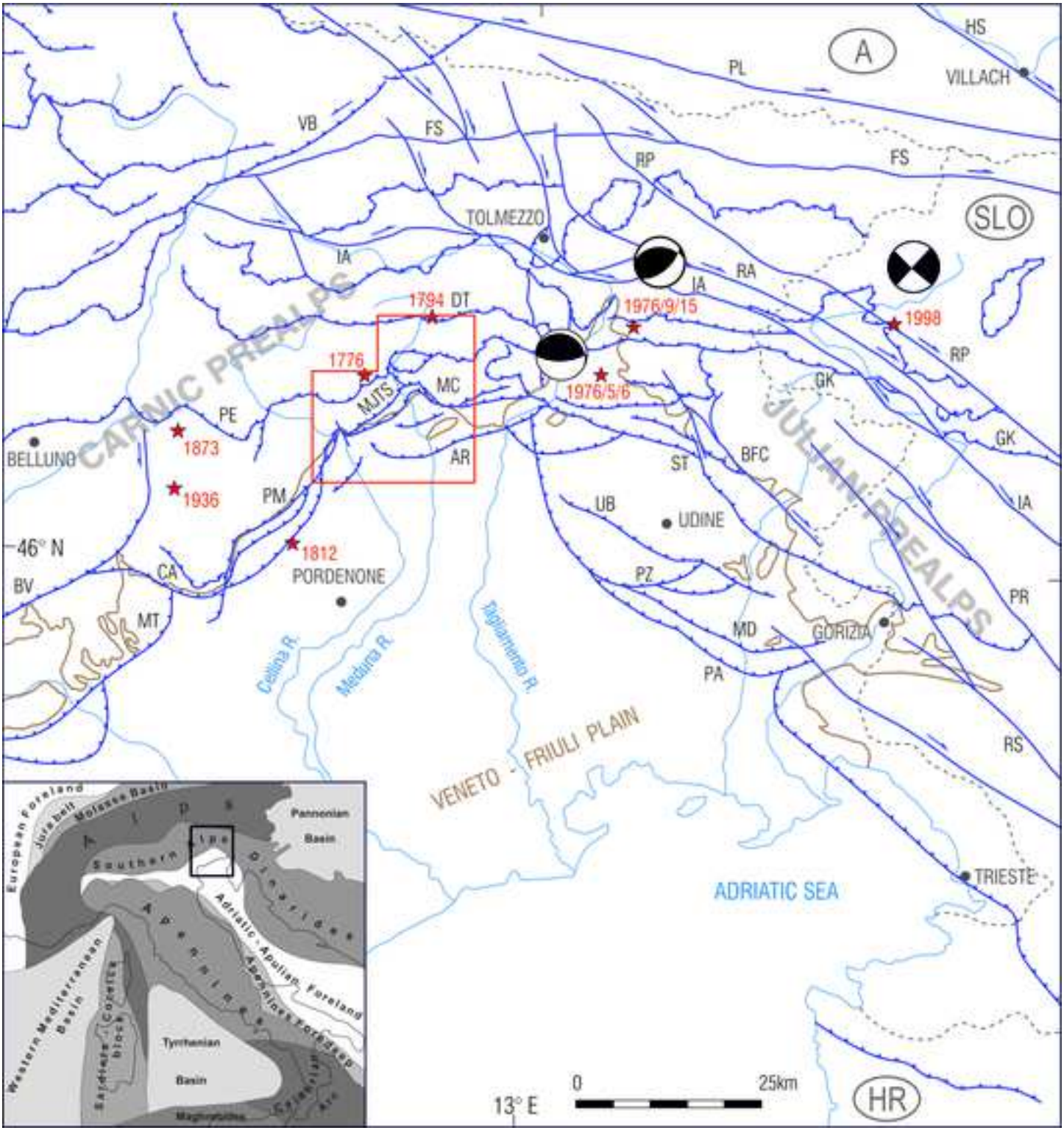

Figure 2

Click here to access/download;Figure (with caption below and on the same page);Figure 2.tif

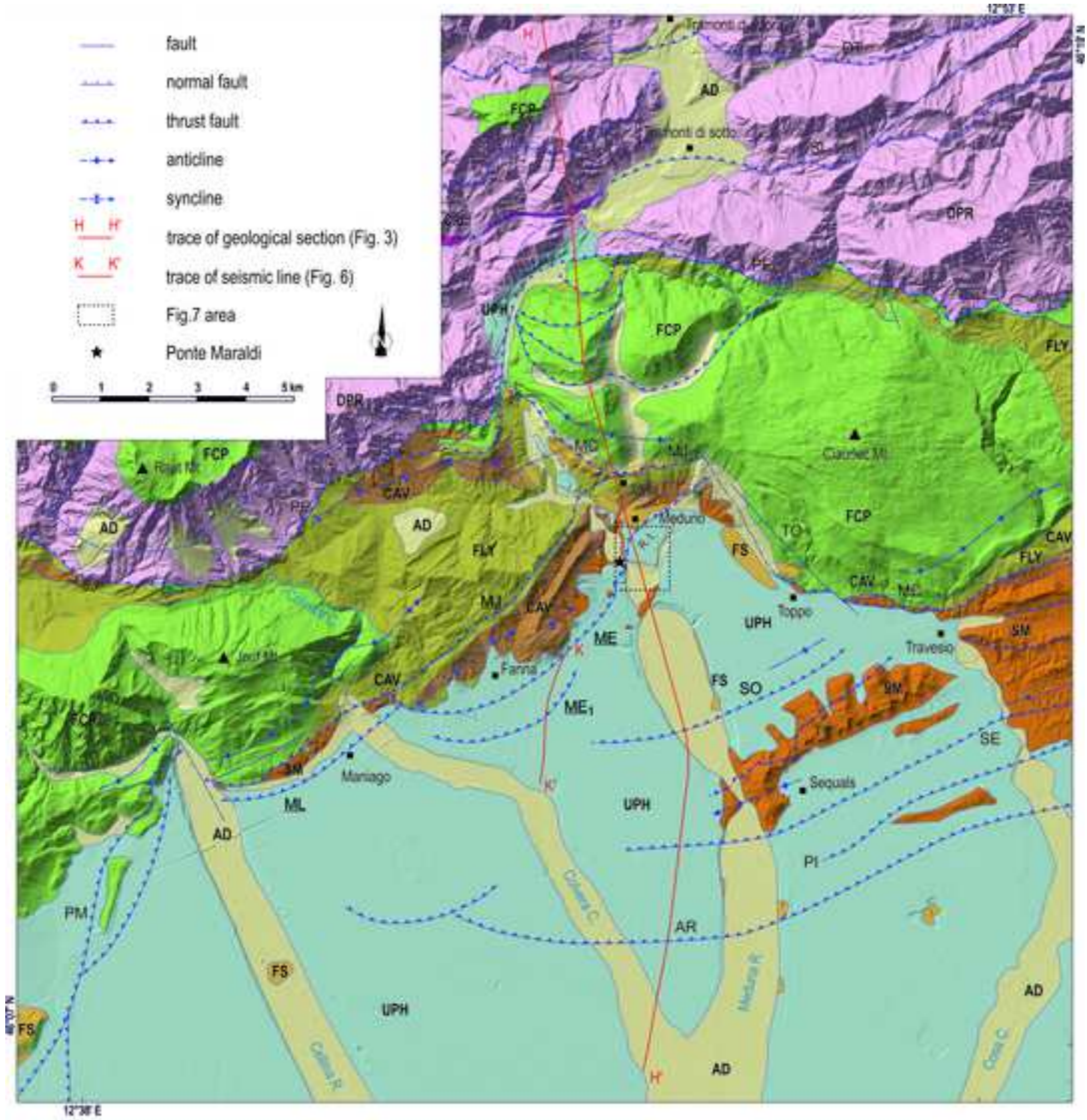

AD: Present alluvial and undifferentiated slope deposits

UPH: Upper Pleistocene (LGM) - Holocene p.p. alluvial and lacustrine deposits

FS: pre-LGM Pliocene-Quaternary alluvial and glacial deposits (Friuli Supersyntem)

Miocene Molassa **SM**: Serravalian-Messinian units
CAV: Aquitanian - Langhian Cavanella Group

FLY: emipelagic and turbiditic deposits (Lower Eocene)

FCP: Lower Jurassic - Upper Cretaceous carbonate platforms

DPR: Upper Triassic carbonate platforms

C.u: Carnian Travenanzes fm. (Carnian unconformity)

Figure 3

Click here to access/download;Figure (with caption below and on the same page);Figure 3 .tif

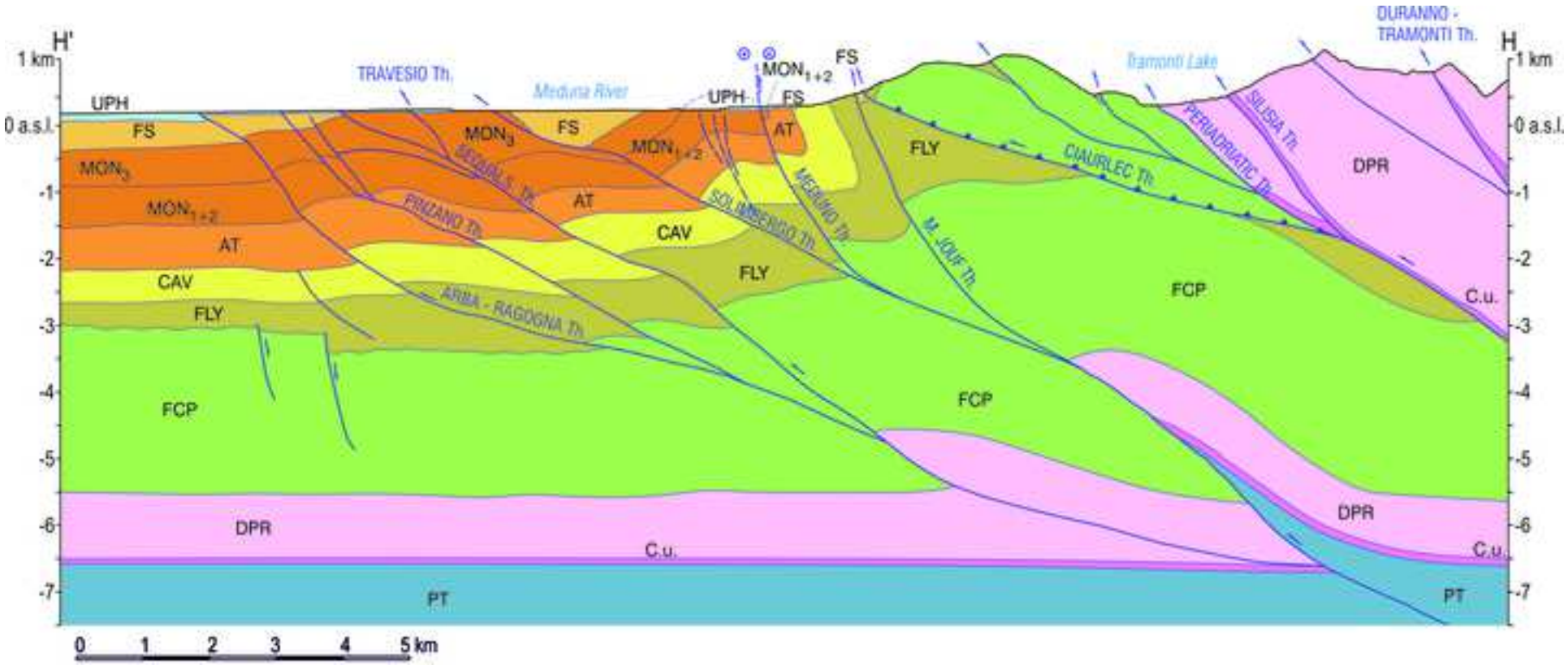

Figure 4

Click here to access/download;Figure (with caption below and on the same page);Figure 4.tif

Figure 5

Click here to access/download;Figure (with caption below and on the same page);Figure 5.tif

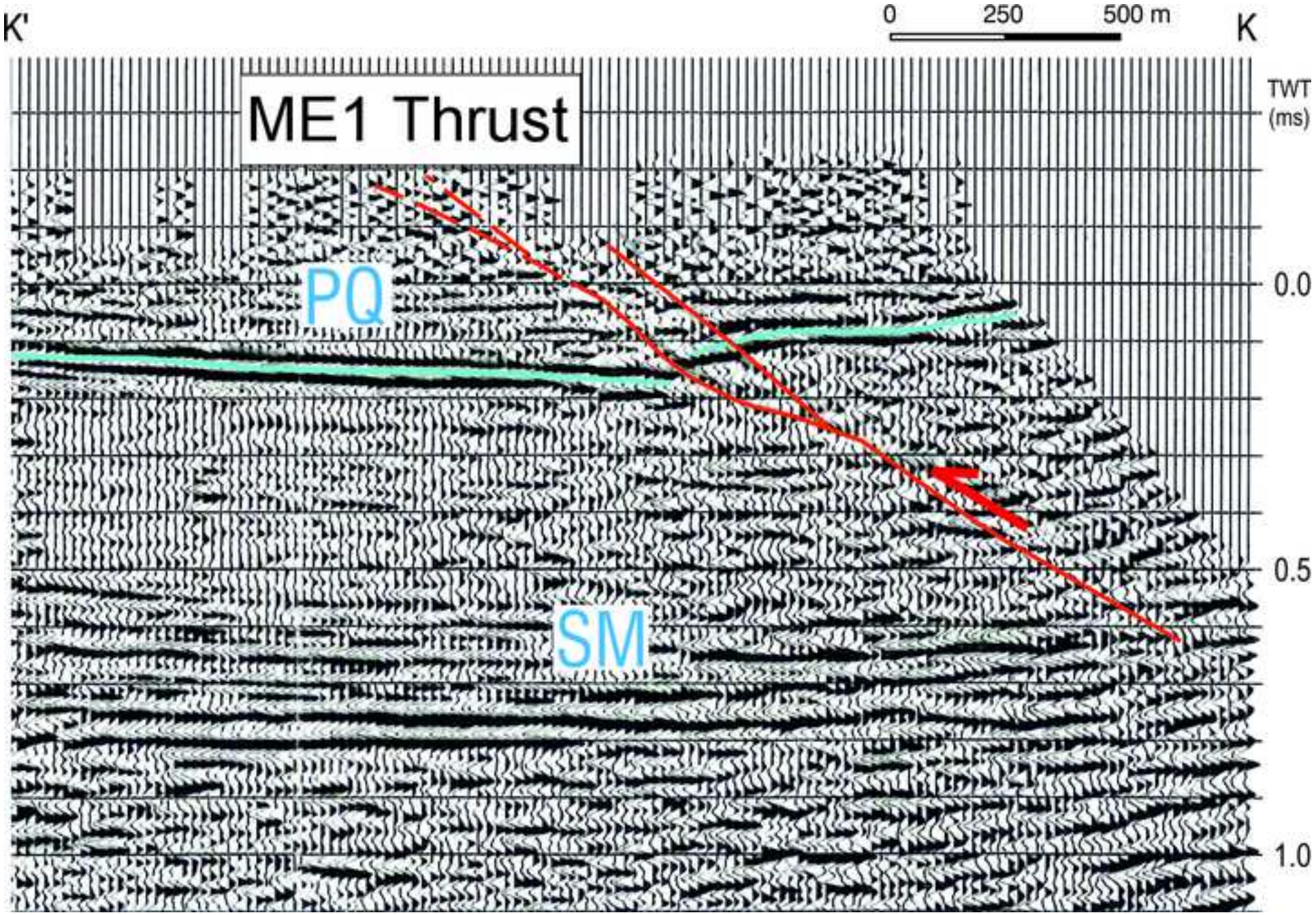

Figure 6

Click here to access/download;Figure (with caption below and on the same page);Figure 6.tif

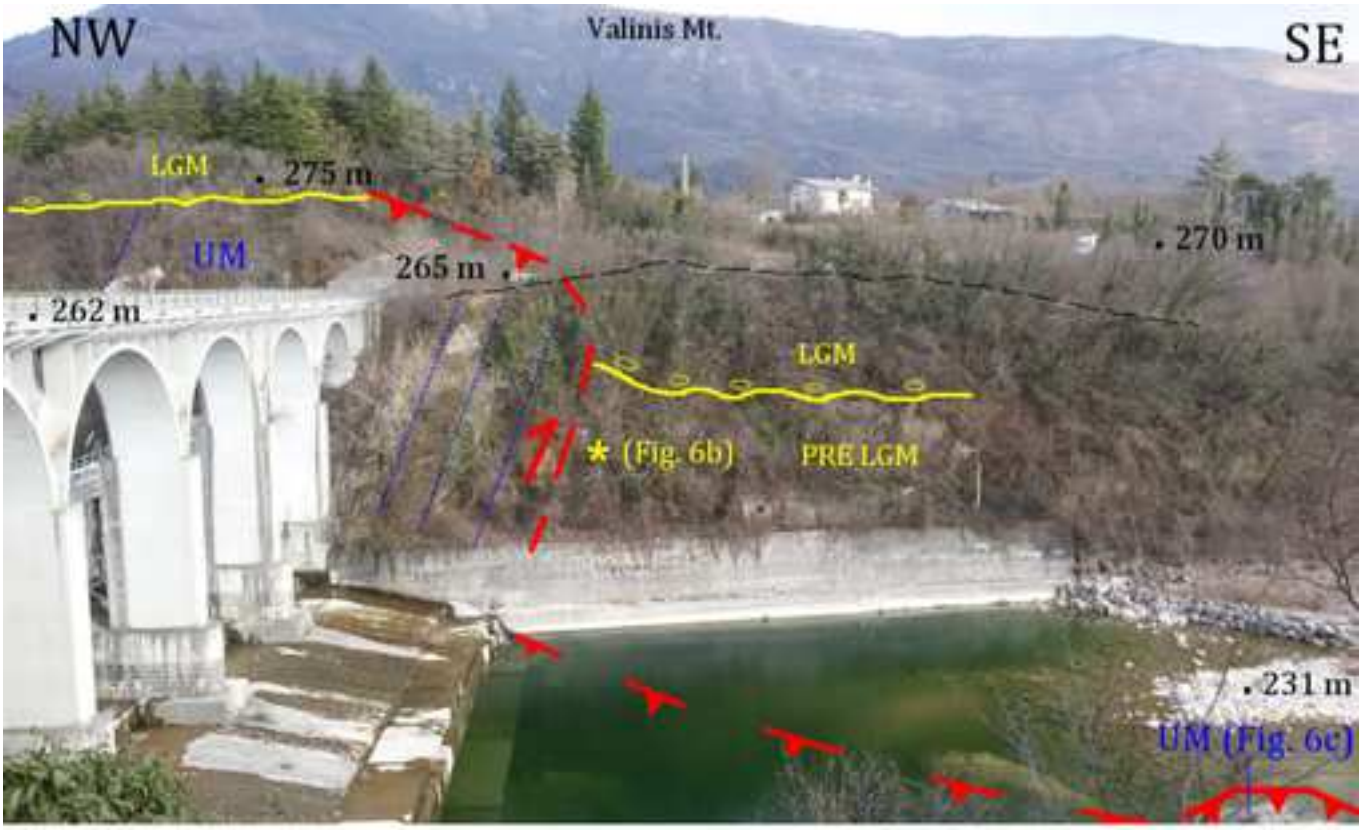

a

b

c

Figure 7

Click here to access/download;Figure (with caption below and on the same page);Figure 7.tif

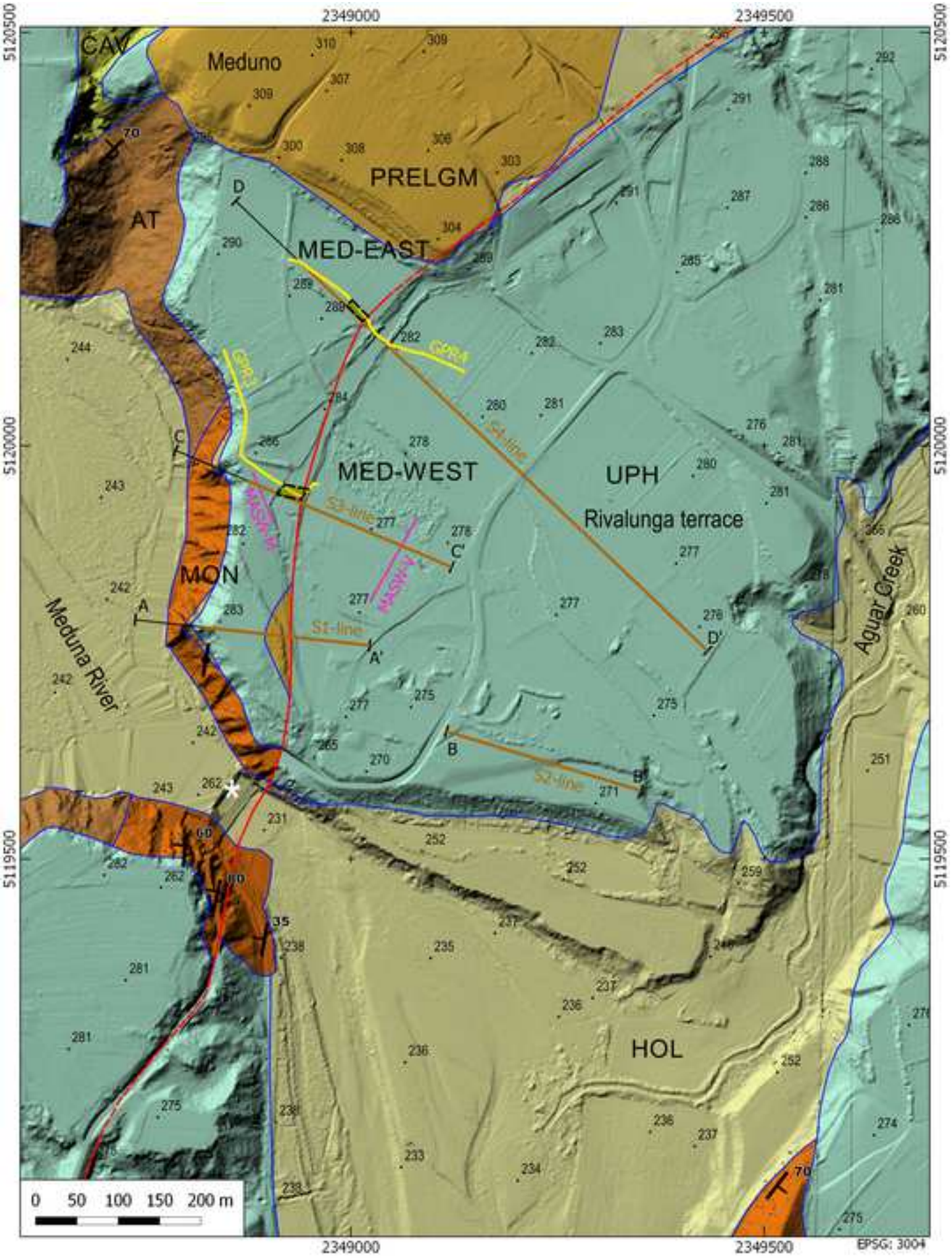

Figure 8

Click here to access/download;Figure (with caption below and on the same page);Figure 8.tif

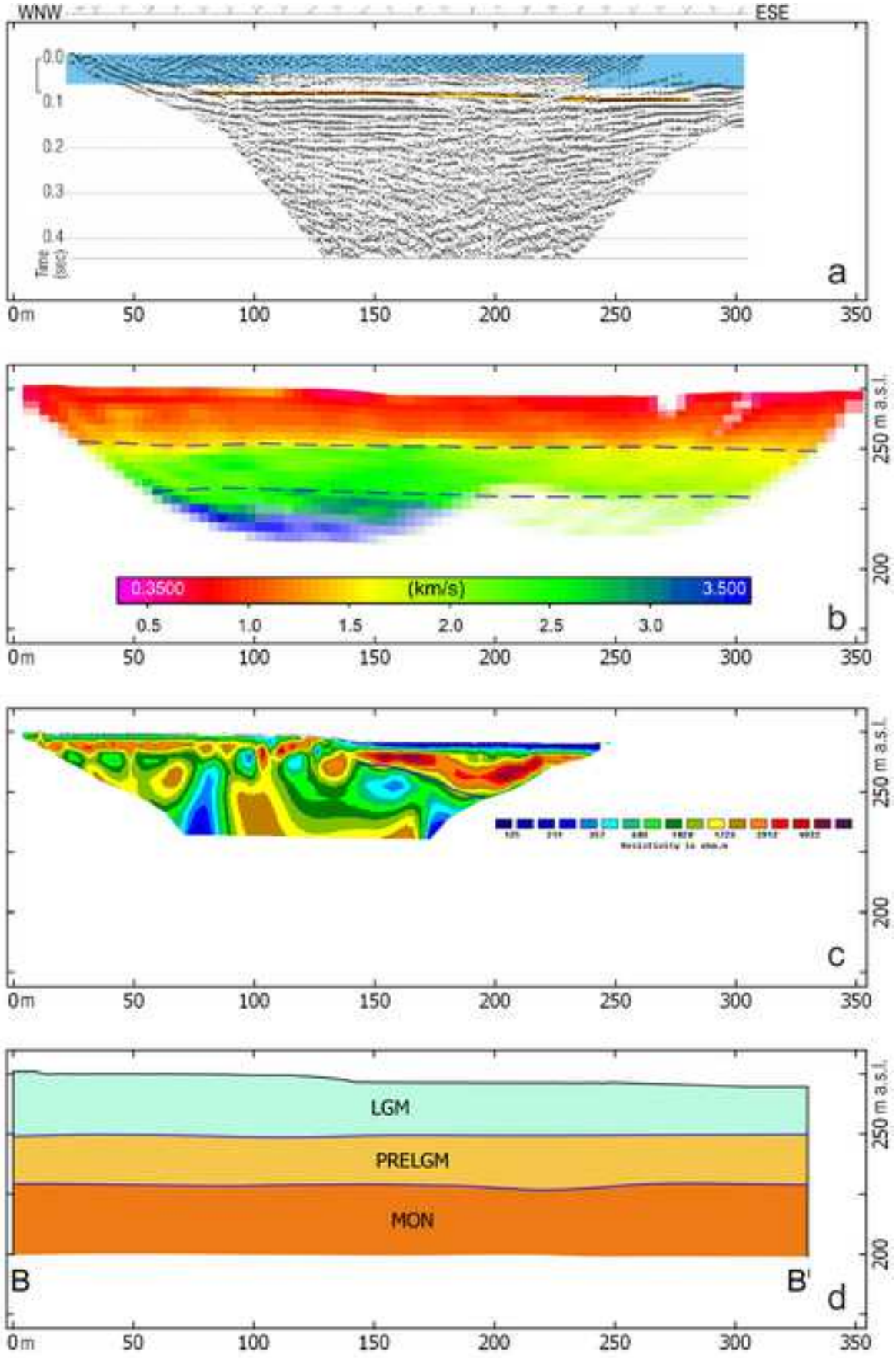

Figure 9

Click here to access/download;Figure (with caption below and on the same page);Figure 9.tif

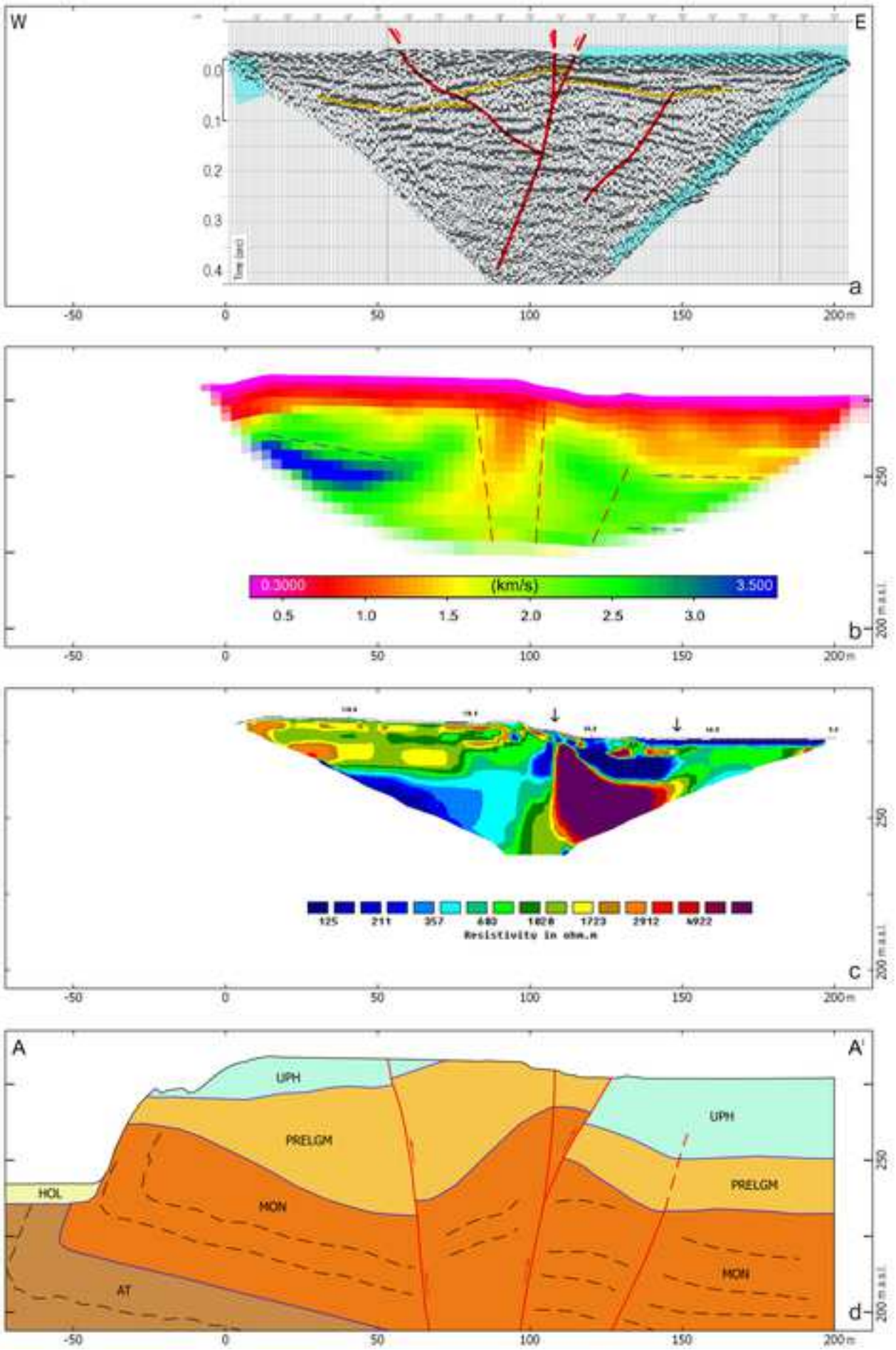

Figure 10

Click here to access/download;Figure (with caption below and on the same page);Figure 10.tif

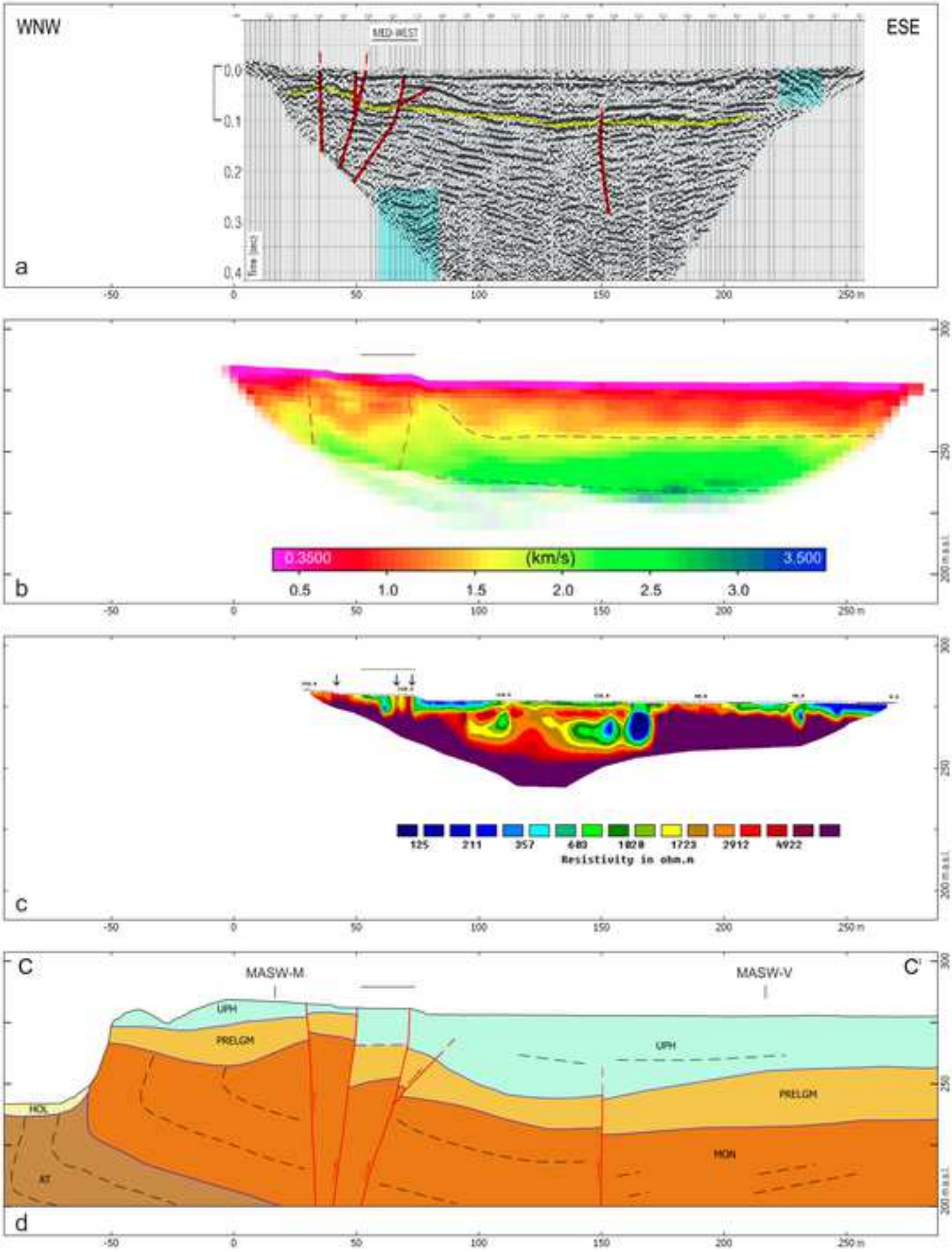

Figure 11

Click here to access/download;Figure (with caption below and on the same page);Figure 11.tif

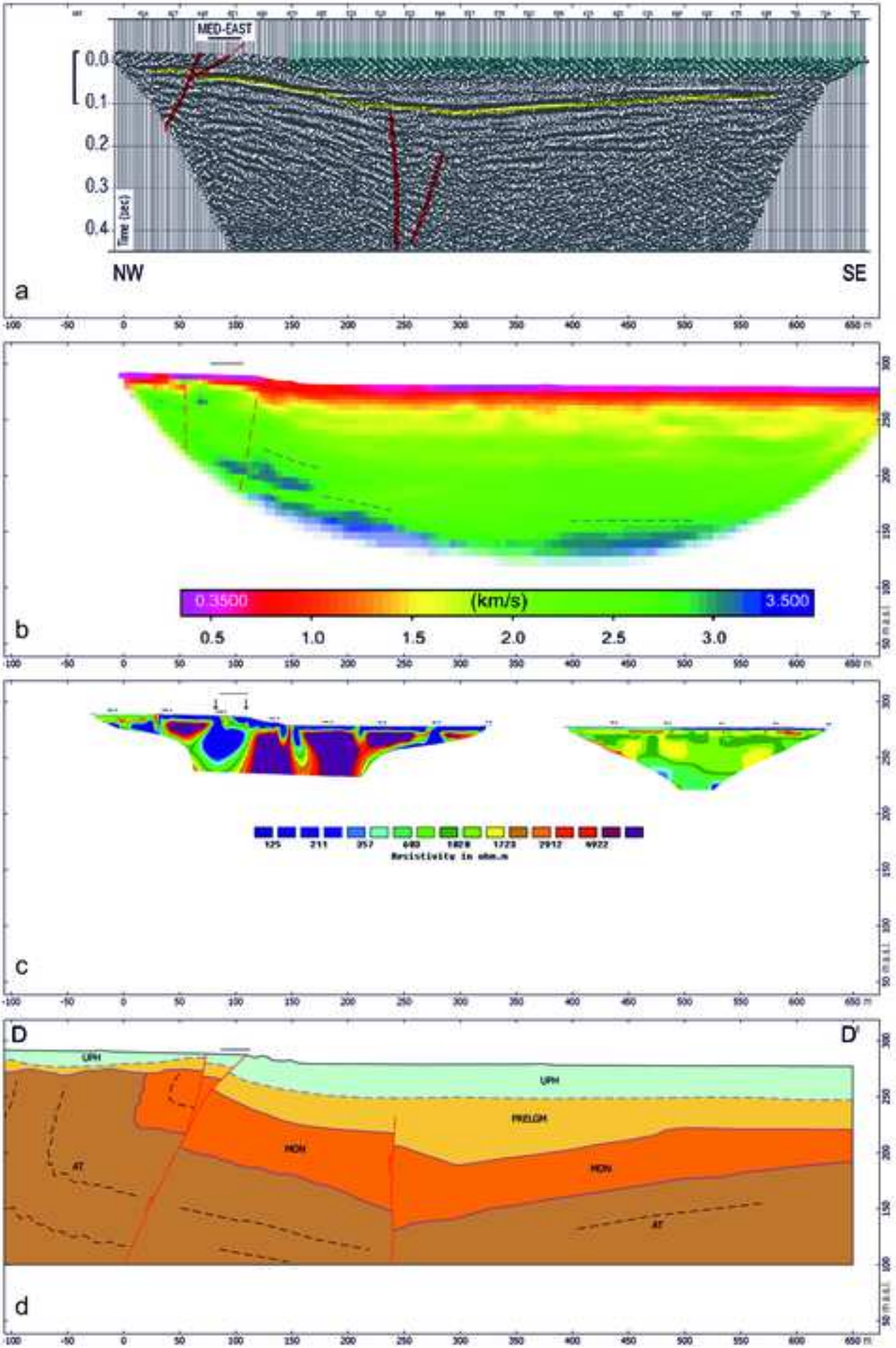

Figure 12

Click here to access/download;Figure (with caption below and on the same page);Figure 12.tif

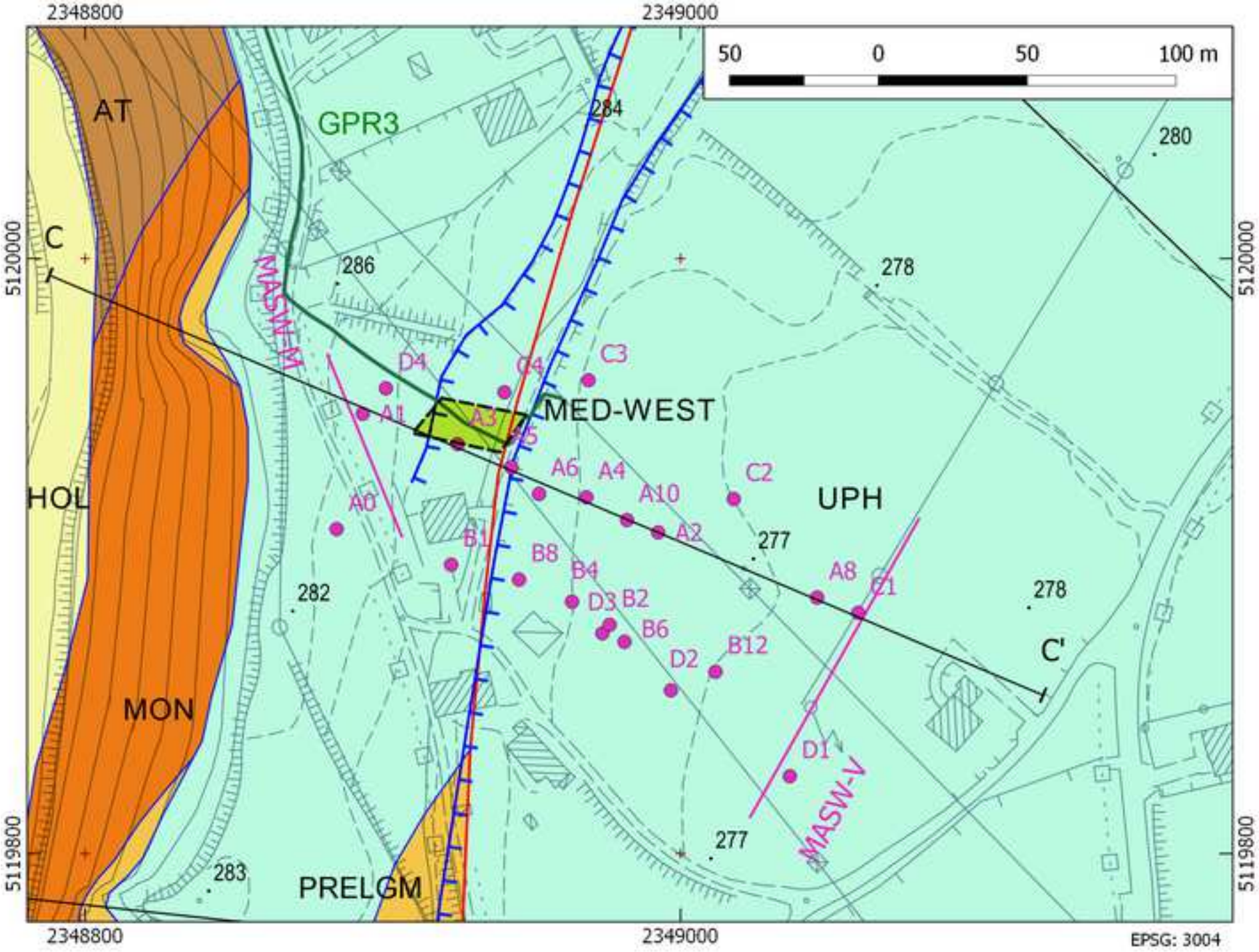

Figure 13

Click here to access/download;Figure (with caption below and on the same page);Figure 13.tif

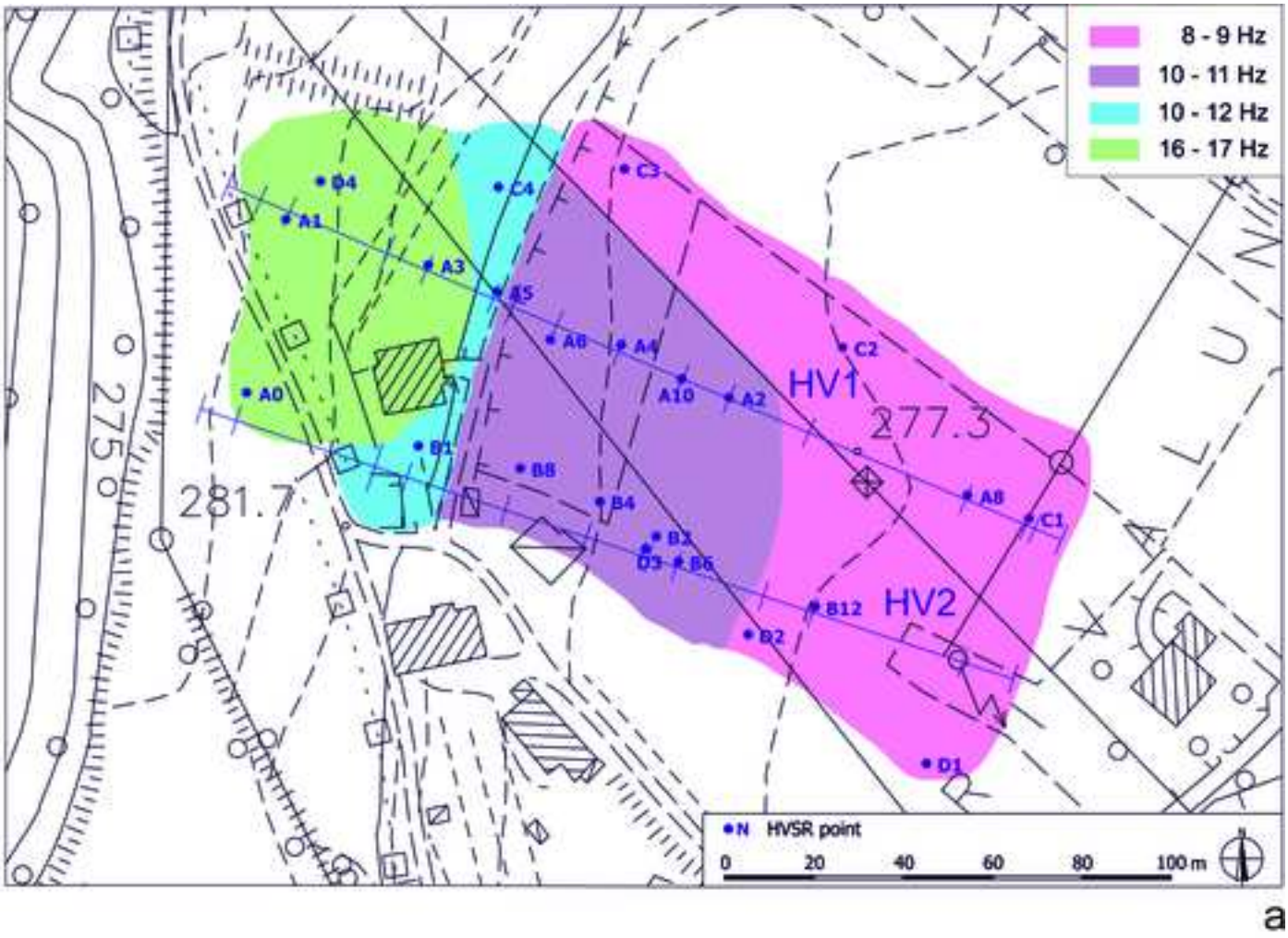

a

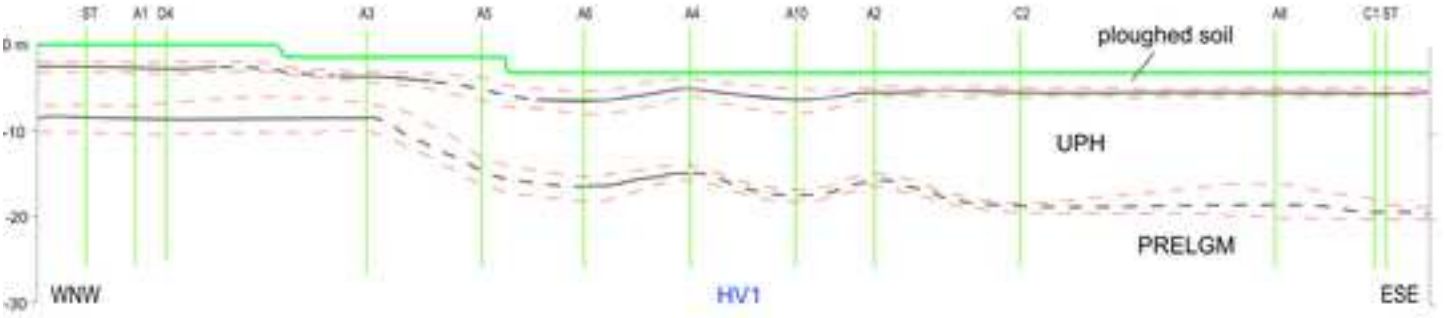

b

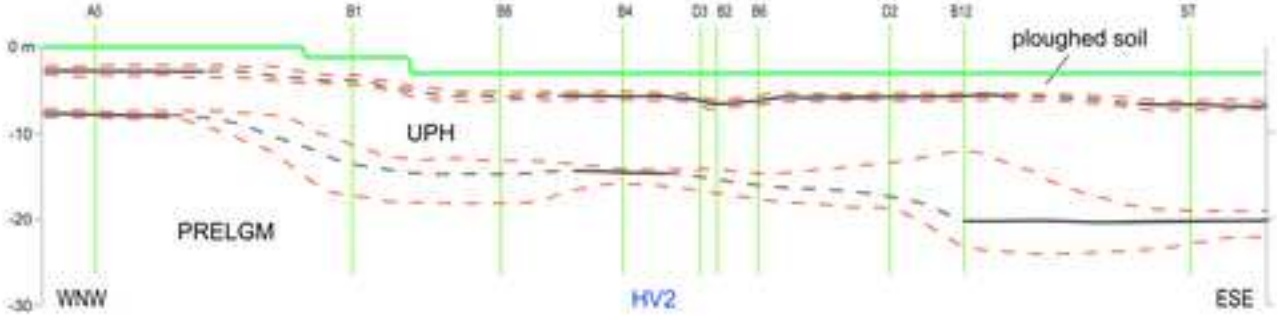

c

Figure 14

Click here to access/download;Figure (with caption below and on the same page);Figure 14.tif

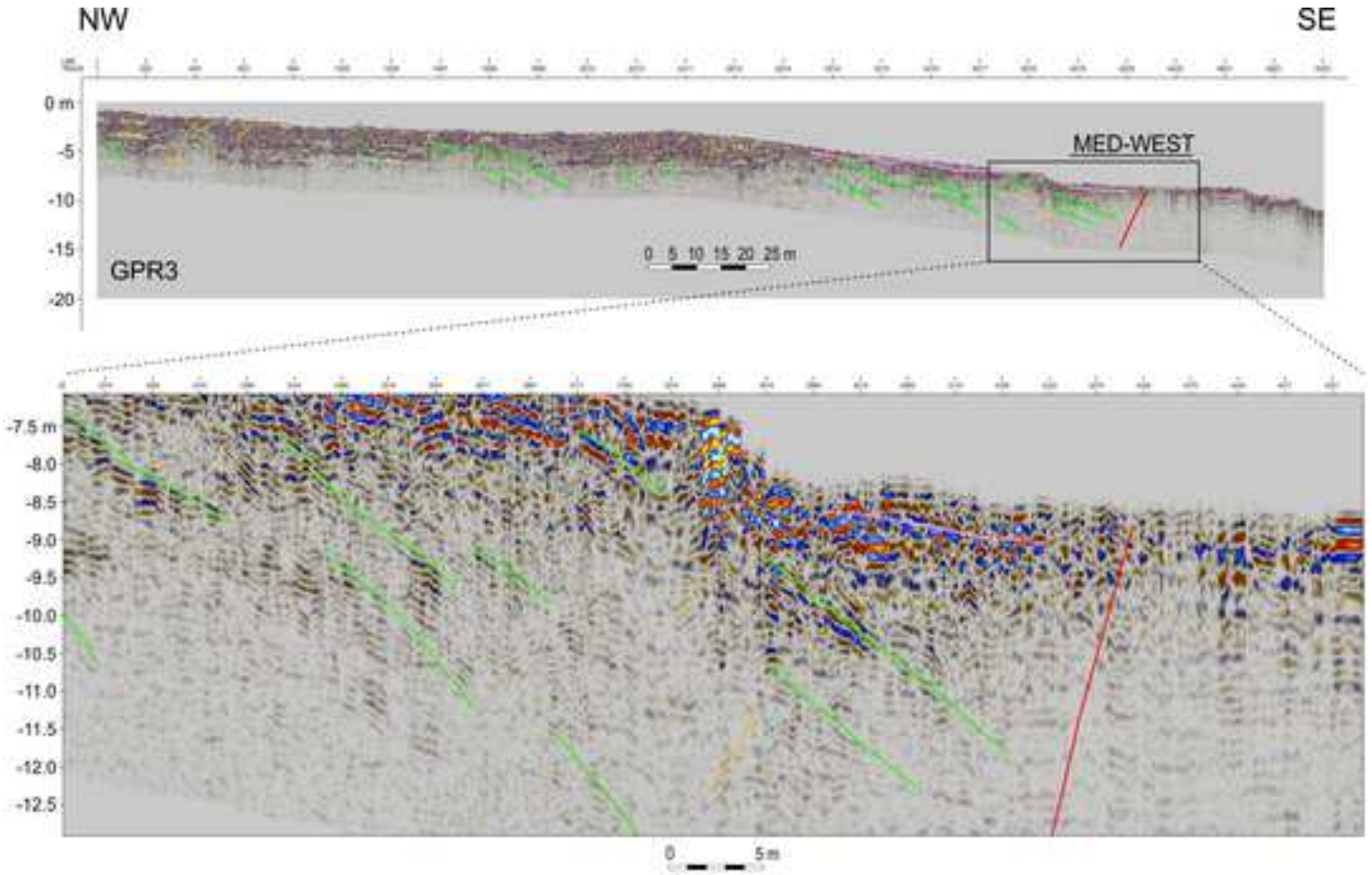

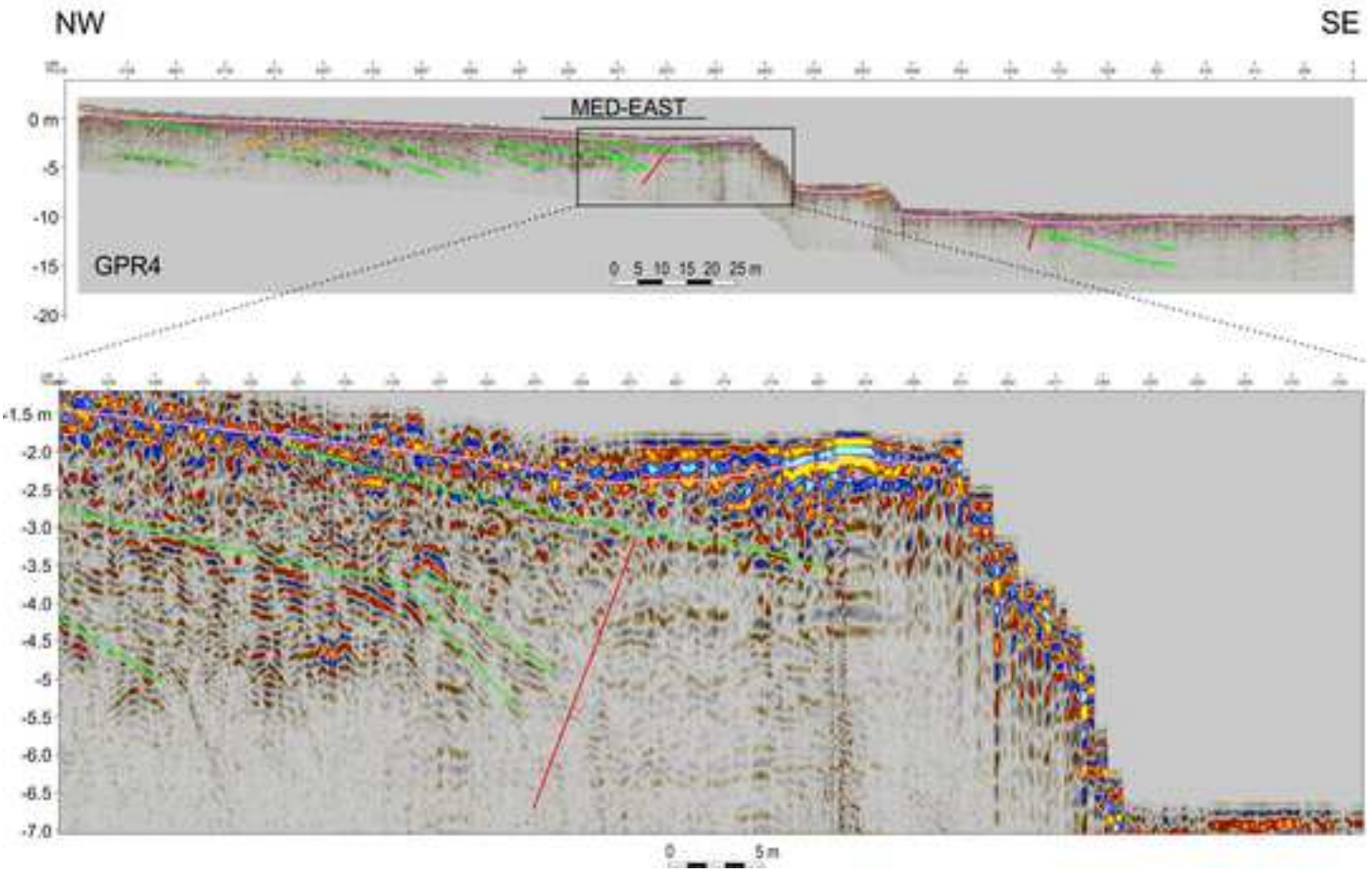

Figure 15

Click here to access/download;Figure (with caption below and on the same page);Figure 15.jpg

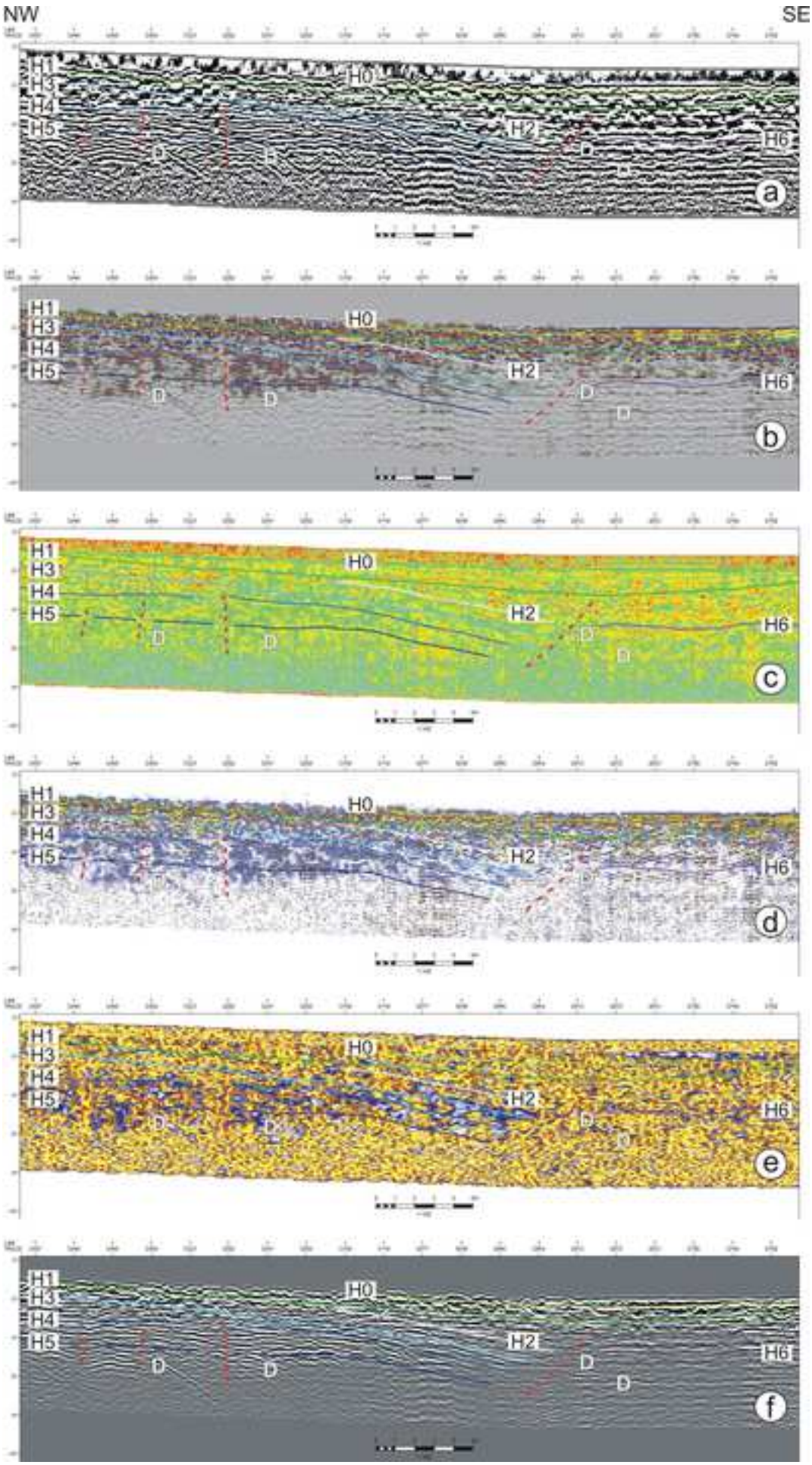

Figure 16

Click here to access/download;Figure (with caption below and on the same page);Figure 16.tif

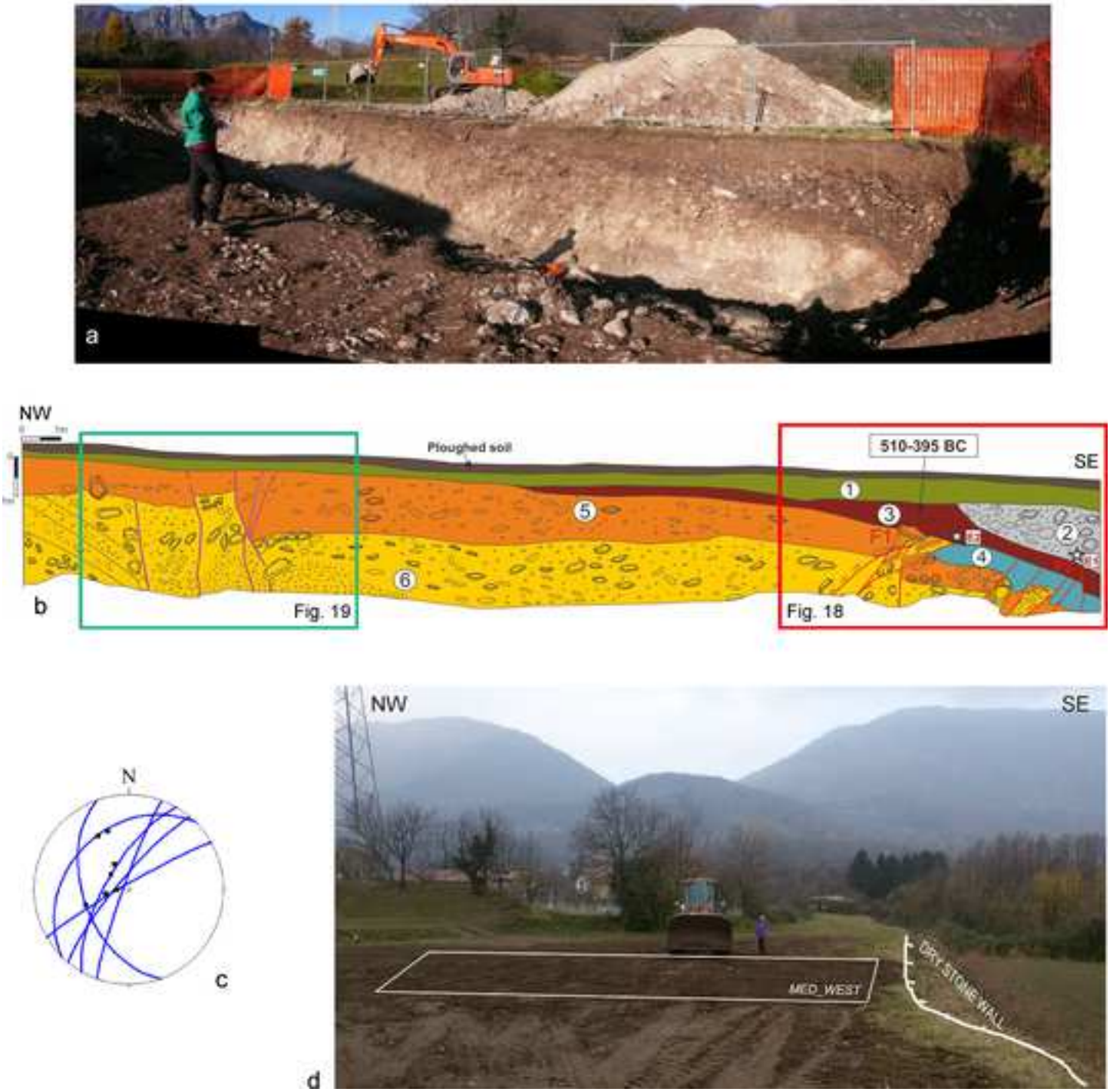

Figure 17

Click here to access/download;Figure (with caption below and on the same page);Figure 17.tif

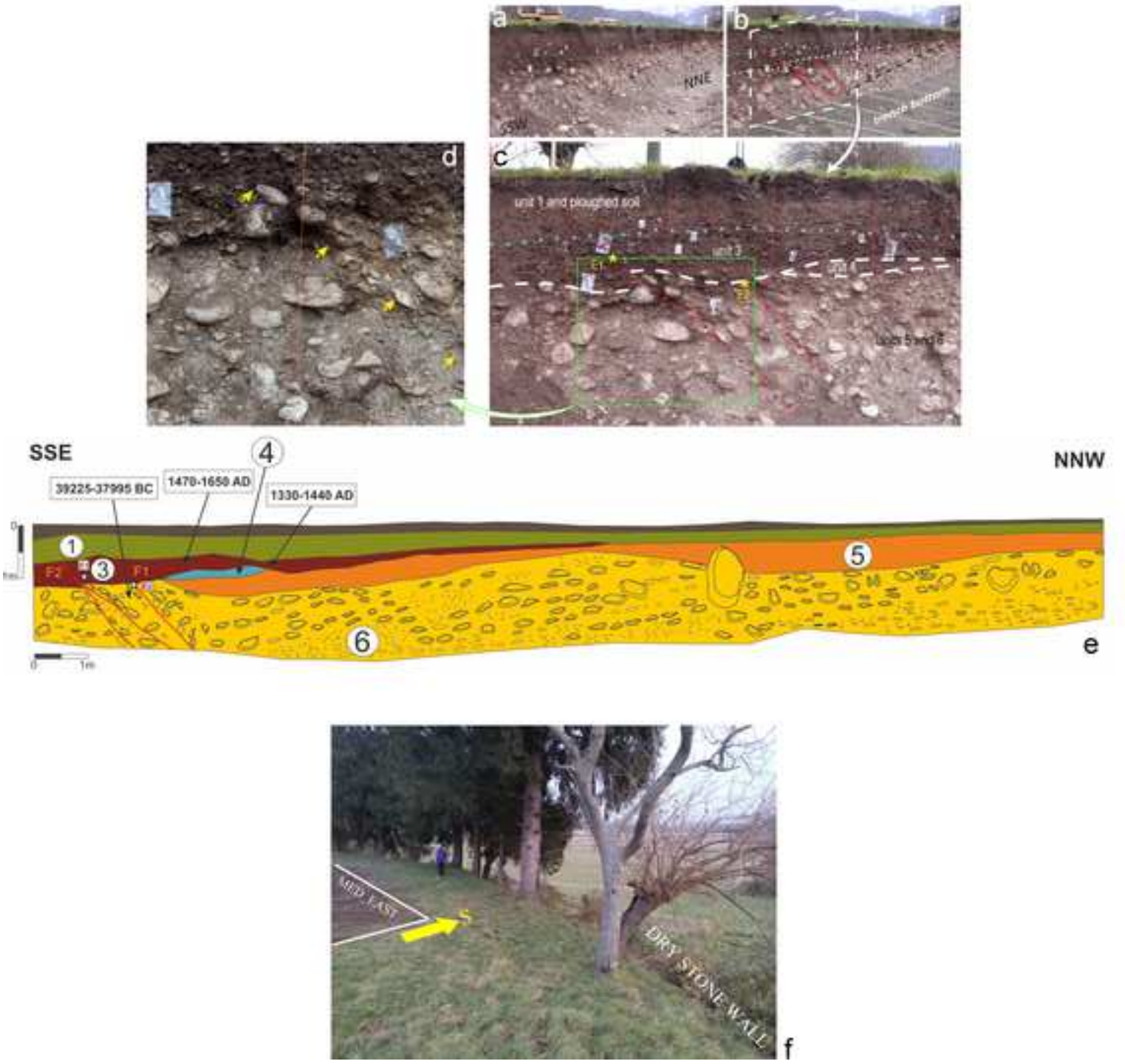

Figure 18

Click here to access/download;Figure (with caption below and on the same page);Figure 18.tif

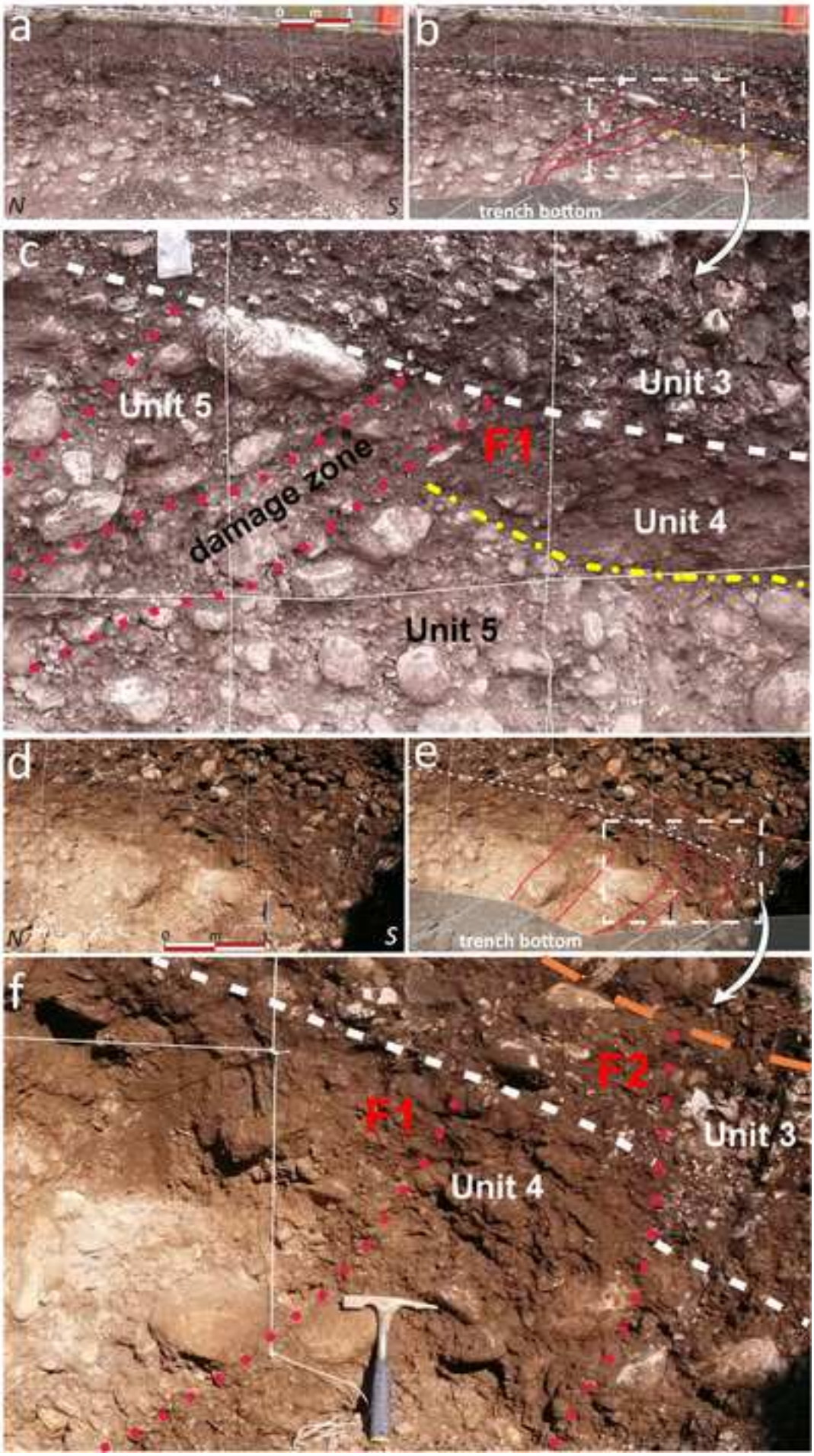

Figure 19

Click here to access/download;Figure (with caption below and on the same page);Figure 19.tif

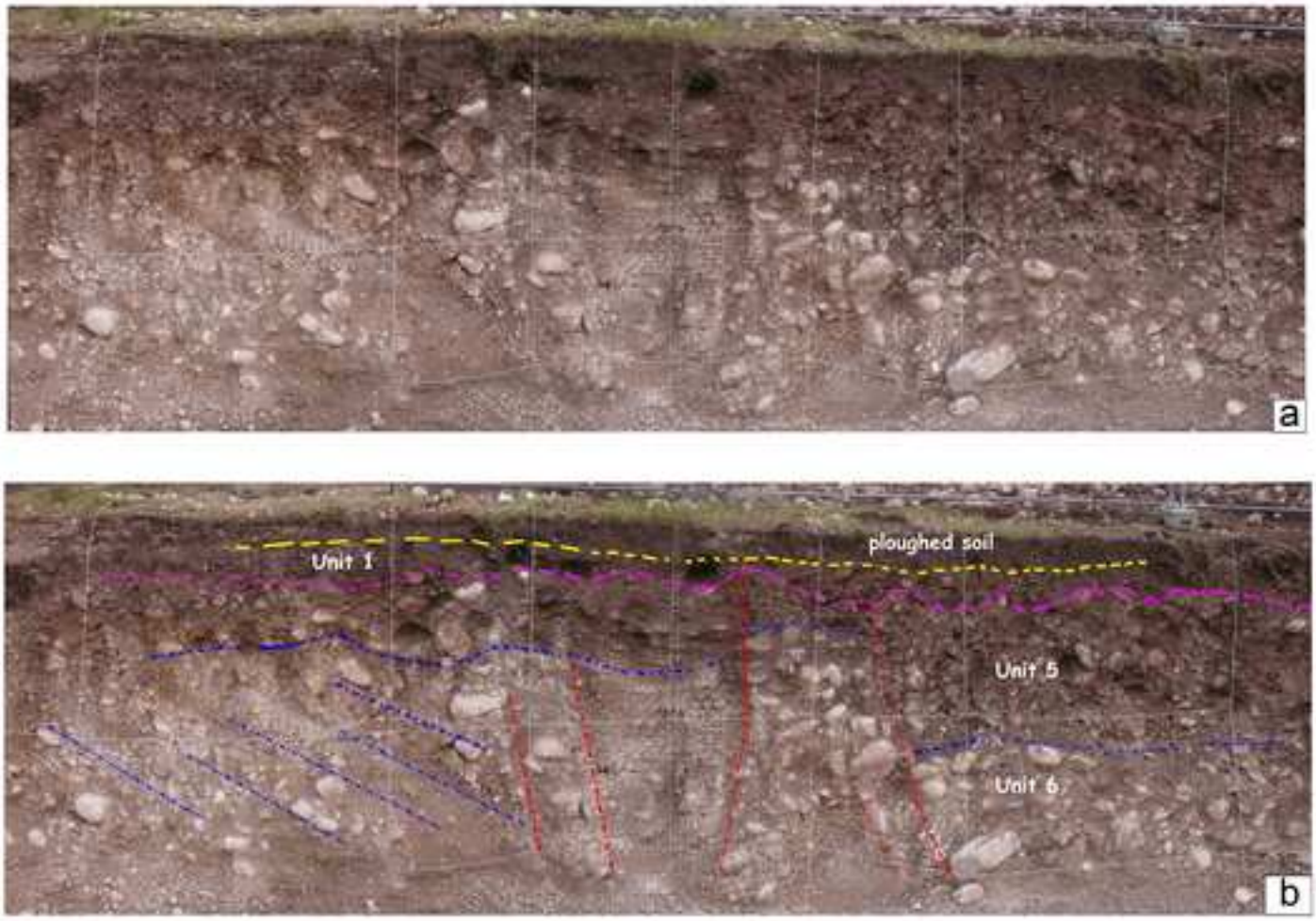

Figure 20

Click here to access/download;Figure (with caption below and on the same page);Figure 20.tif